Egypt. J. Chem. **Vol. 68**, SI: Z. M. Nofal, pp. 705 - 739 (2025)

Egyptian Journal of Chemistry

http://ejchem.journals.ekb.eg/

Removal of Cu, Cr, Zn, and Pb from Wastewater by Using a Composite of Chitosan and Metal Organic Framework Mil (53) Fe

Sameh M. Fouad [1], Nada M. Aboeleneen [2], Hussein Oraby [1], Nabil M. Abd-ElMonem [3], Faisal H. Sorour *[4]

[1]*Chemical Engineering Department, Military Technical College, Cairo, 11766, Egypt*

[2]*Chemical Engineering Department, Higher Institute of Engineering and Technology, New Damietta, 34517, Egypt*

[3]*Chemical Engineering Department, Faculty of Engineering, Cairo University, 12613, Egypt*

[4]*Chemical Engineering Department, Canal High Institute for Engineering and Technology, Suez, 43522, Egypt*

Abstract

Wastewater exhibits elevated concentrations of heavy metals that pose significant risks to human, animal, and plant health. Using chitosan and metal-organic framework (MOF MIL (53) Fe), a composite was synthesized by hydrothermal methods to eliminate certain heavy metals (Cu, Cr, Zn, and Pb) from wastewater. The surface areas of chitosan, MOF, and their composite were evaluated using the Brunauer-Emmett-Teller (BET) method. The measured surface areas were 16.5 m²/g for chitosan, 3.5 m²/g for MOF, and 109.038 m²/g for the composite, respectively. The morphological analysis was made using a scanning electron microscope (SEM-TEM); the average size particles of chitosan, MOF, and composite were observed to be (500 to 20) µm, (50 to 10) µm, and (50 to 10) µm, respectively. The removal efficiency and the adsorption capacity for chitosan, MOF, and composite were studied at pH 7, adsorbent dose 0.3 g, initial concentration 5 ppm, and contact time 60 minutes. The mean removal efficiencies were 97.35% for chitosan, 97.45% for MOF, and 98.145% for the chitosan/MOF composite. The mean adsorption capacities were 0.81 mg/g for chitosan, 0.811 mg/g for MOF, and 0.817 mg/g for the chitosan/MOF composite. The Freundlich model more accurately describes the sorption of Cu, Cr, Zn, and Pb compared to the Langmuir model. The manufacturing process of 10 grams of chitosan costs about 70 Egyptian pounds, while 10 grams of MOF costs 700 Egyptian pounds and 10 grams of composite costs 250 Egyptian pounds.

Keywords: Adsorption; Brunauer-Emmett-Teller (BET); Cost-Effectiveness; Freundlich Isotherm; Hydrothermal Synthesis; Langmuir model.

1. Introduction

Water is an essential natural resource critical to the survival of humans, animals, and plants. Freshwater constitutes only 2.5% of the global water supply, and the proportion of accessible freshwater is significantly limited as a result of its unequal distribution. According to the 2021 World Water Development Report published by UNESCO, this disparity poses a significant challenge to sustainable water management worldwide [1, 2]. Over 80% of sewage generated by human activities is discharged into seas, rivers, and oceans without treatment, leading to significant environmental pollution. More than 80% of global diseases and 50% of child deaths are linked to poor water quality [3]. Insufficient water sanitation facilitates the transmission of diseases like trachoma, cholera, schistosomiasis, and helminthiasis. Moreover, polluted water, which contributes to inadequate environmental sanitation, induces gastrointestinal illnesses, hinders nutritional absorption, and results in malnutrition [1, 4].

The Environmental Protection Agency (EPA) of the United States classifies water pollutants into six categories, such as plant nutrients, pathogens, sediment, toxic organic chemicals, toxic heavy metals, and thermal pollutants [5-7]. Heavy metals such as manganese (Mn), chromium (Cr), iron (Fe), cobalt (Co), nickel (Ni), copper (Cu), zinc (Zn), arsenic (As), molybdenum (Mo), cadmium (Cd), mercury (Hg), and lead (Pb) are naturally present in soil and can also be byproducts of agriculture, mining, industrial wastes, vehicle exhausts, lead batteries, paint products, treated woods, aging water supply infrastructures, and microplastics wastes in oceans [8]. Heavy metals present in wastewater often derive from sources such as fertilizers, herbicides, and diverse industrial operations, including plating, tanning, dyeing, textile production, and electrochemical processes [9-13]. Copper, zinc, and lead can contribute to major health problems such as kidney damage, liver damage, convulsions, cramps, vomiting, CNS disturbances, and even death in severe poisoning cases [14-18].

As potable water supplies continue to diminish, wastewater treatment has surfaced as a viable compensatory approach,

*Corresponding author e-mail: sorourfh@outlook.com.; (Faisal H. Sorour).

Received date 10 March 2025; Revised date 05 June 2025; Accepted date 12 June 2025

DOI: 10.21608/ejchem.2025.358788.11275

resulting in several scientific and technological innovations in treatment methods. Conventional wastewater treatment technologies include chemical precipitation, membrane filtration, and ion exchange. The chemical precipitation method is commonly employed because of its straightforward approach. While membrane filtration is also efficient, it involves high initial operational costs. The ion exchange method works by exchanging anions and cations in the solution medium; however, it is useless in concentrated metal solutions. Many of these methods share similar drawbacks, such as high expenses, incomplete removal of specific ions, and the production of sludge, which incurs additional costs for disposal.

In recent years, alternative treatment approaches, including photocatalysis, electrochemical techniques, flotation, coagulation, and adsorption, have gained considerable interest, as conventional water treatment systems rely on centralized plants that distribute treated water via dedicated distribution networks, while alternative methods offer decentralized, cost-effective, and environmentally friendly solutions that can be implemented closer to pollution sources, reducing energy demand and infrastructure requirements. It should be noted that the treatment process may differ from one country to another, according to many factors such as the population, weather conditions, and the technology used [19, 20].

Regarding heavy metal elimination from wastewater, many methods are available, such as ion exchange, reverse osmosis, and precipitation, which are important techniques for removing heavy metals chemically [21-25]. Many of these methods have limitations, such as high cost, time consumption, logistic problems, and mechanical involvement.

As depicted in Figure 1, chitosan is a biodegradable and non-toxic polymer derived from the deacetylation of chitin. Chitin is a natural polysaccharide commonly found in the exoskeletons of crustaceans, such as shrimp, and in insects [26]. It has been widely employed in recent decades due to its multiple functional uses, and it is one of the most functionally versatile adsorbents since it comprises hydroxyl (-OH) and amine ($-NH_2$) groups. It also possesses antimicrobial capabilities, high cationic charge density, and a cellulose structure that may be used in a variety of applications. While insoluble in most solvents, chitosan exhibits slight solubility in diluted organic acids, including acetic, lactic, malic, formic, and succinic acids [27]. Chitosan was used for water treatment and purification in the past as an adsorbent or a flocculent and coagulant for removing heavy metals from dyes, pesticides, and biological contaminants from different types of water [28].

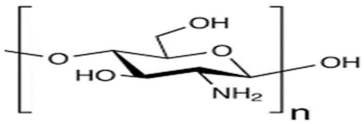

Fig. 1. Structure of chitosan.

A novel class of highly tunable hybrid materials is Metal-Organic Frameworks (MOFs) seen in Fig. 2. These crystalline compounds are composed of metal ions or clusters coordinated with rigid organic molecules, forming one-dimensional (1D), two-dimensional (2D), or three-dimensional (3D) structures with varying porosity. They are formed from metal ions joined by organic bridging ligands and have received substantial interest because of their large surface area, open crystalline structure, and their abundance of adjustable organic groups that allow for easy adjustment of pore size [29]. Additionally, their application in removing pollutants, such as heavy metals, from water has further increased their appeal [30-32].

MOF MIL 53 (Fe) is an organic-inorganic hybrid material composed of iron and terephthalate ligands generating a three-dimensional (3D) lattice structure with high thermal and hydrolytic stability [33]. MOFs may be integrated into diverse materials such as nanomaterials and functional materials. They have the potential to be changed to porous carbon materials and metal oxides/sulphides by several processes such as calcination, sulfurization, and chemical etching.

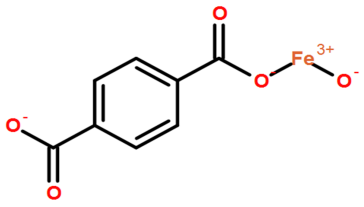

Fig. 2. Structure of MOF MIL (53) Fe.

Chitosan-coated metal-organic frameworks are chemically and thermally stable, recyclable, and have a high adsorption capacity. It can be synthesized by the situ growth method and crosslinking between chitosan and metal-organic framework and used to eliminate heavy metals such as Cu, Cr, Zn, and Pb from wastewater by a very simple process [34, 35].

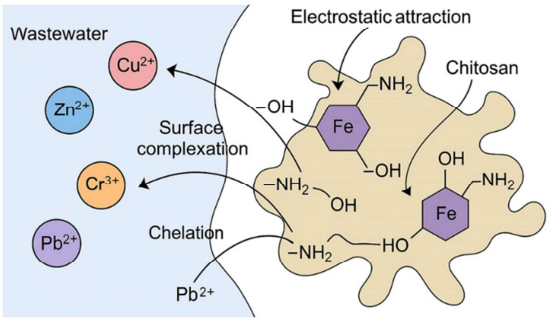

Fig. 3. Graphical summary of the heavy metal adsorption by the composite.

The goal of this research is to create composite hydrogel spheres from MIL-53(Fe) and chitosan by covering chitosan with MIL-53(Fe). The structural and physicochemical characteristics of the composite will be determined utilizing a variety of methods, including SEM, FTIR, XRD, TGA, BET, and zeta potential analysis. Subsequently, the composite will be used to remove heavy metals from wastewater.

2. Materials and Methods

2.1. Materials

All of the chemical reagents utilized in this study were analytical grade, including a stock mix solution of 1000 mg/l of copper, chromium, zinc, and lead with a purity of 99.9%, 98% sodium hydroxide, 68% nitric acid, and 36% hydrochloric acid, all obtained from Accustandard Company at New Haven in the USA. All the aqueous solutions were prepared by using high-grade ultrapure water with resistivity (18.2) MΩ, the ultrapure water produced from the Millipore Direct–Q–UV device, France. Also, iron (III) chloride hexahydrate 97%, terephthalic acid 98%, N,N-dimethyl formamide 99.8%, acetic acid 99%, sodium tripolyphosphate 80%, methanol 99.9%, and acetone 99.5% all were received from Sigma Aldrich company.

2.2. Methods

2.2.1. Preparation of adsorbents

Chitosan was prepared from shrimp shells using 3 kg of Egyptian shrimp from the local market. The shells were dried at 40°C in a ZRD-7080 made in the USA oven for 48 hours, then the dried shells were ground and stored in a plastic bottle at room temperature. The demineralization process of shrimp shells is then done by soaking in 5% HCl for 24 hours with a solid-to-ratio of 1:6. After 24 hours, the soft shells were rinsed with water to eliminate acid and calcium chloride, followed by drying in an oven at 60°C. The procedure was repeated using a 10% HCl solution to verify that the shells were completely demineralized, yielding 29.5 grams. The demineralized shells were then deproteinized using a 5% NaOH solution for 48 hours at 60°C, with a solid-to-solvent ratio of 1:10. The residue was washed with distilled water to remove NaOH and dried for 48 hours, yielding 22.38 grams of chitin. The deacetylation method, which transforms chitin to chitosan by removing the acetyl group, entailed cleaning the decalcified chitin with distilled water before transferring it to a 60% sodium hydroxide solution. The solution was microwaved for two hours to guarantee full deacetylation. The resulting material was washed with distilled water and dried at 60°C for 2 hours to provide 15.37 grams of chitosan [36-38].

MOF MIL (53) Fe was synthesized as 10.5 g of iron (III) chloride hexahydrate ($FeCl_3 \cdot 6H_2O$) was mixed with 5.2 g of 1,4-benzenedicarboxylic acid and 200 ml of N,N-dimethylformamide. The mixture was then agitated for 30 minutes. The mixture then was placed in a Teflon-lined steel autoclave and heated in the oven for 15 hours at 120-130°C. A yellow powder was obtained by filtration and washing with methanol and acetone by a molar ratio of 1:1. MOF MIL53(Fe) was gained by washing with distilled water and dried overnight in the air [39, 40].

MOF/chitosan composite material was prepared by dissolving 0.12 grams of chitosan in 20 ml of 2 wt. % acetic acid, and then 0.18 grams of MOF were added. The mixture then was stirred for 3 hours and 10 wt.% $Na_5P_3O_{10}$ solution was added quickly dropwise with constant stirring at room temperature for 15 min. Finally, the MOF/chitosan composite was collected and rinsed using distilled water, then dried overnight at 80°C [41].

2.2.2. Preparation of heavy metals stock solution

Preparation of five standard concentrations (100, 50, 25, 10, and 5 ppm) of copper, chromium, zinc, and lead by dilution from the 1000 ppm standard with ultrapure water.

2.2.3. Adsorbent characterization

The synthesis process of the chitosan, MOF, and MOF MIL (53) Fe/chitosan composite was analyzed using many techniques. X-ray diffractometer type (X Pert PRO) is used to determine and analyze the phase present in the adsorbent's powders. [42, 43]. Brunauer Emmett Teller (BET) surface area, pore volume, and variation in pore size were measured using the BET instrument model NOVA Station [44, 45]. FTIR spectroscopy was used to identify the adsorbent's functional groups. It was also used to investigate the spectra of the manufactured samples. The resulting infrared spectra were scanned using JASCO FTIR-6200 equipment with a range of (4000:400 cm^{-1}) [46, 47]. Scanning electron microscope (SEM-EDX) is a well-established method for the characterization of materials on both microscale and nanoscale. Energy dispersive analysis of X-rays (EDX) morphological analysis was characterized by a scanning electron microscope type FEI Czech [48]. Bruker Senterra Raman spectroscopy is a new approach for further characterization and detection of molecular features in many processes. The frequency accuracy is ~0.1 cm^{-1}, and the spectral resolution is <3 cm^{-1}. It operates with three laser excitation wavelengths: 785, 633, and 532 nm [49]. Raman spectroscopy is utilized to explain the chemical structure and crystalline nature of nanomaterials to distinguish domain size, bonding type, and internal stress in crystalline and amorphous carbon material. Transmission electron microscopy (TEM) is a key technique for morphological and compositional characterization of materials from nanometer to micrometer scales [50-52]. The Zeta Potential Horbia Scientific SZ-100 V2 instrument measures particle size and particle distribution width using dynamic light scattering (DLS) analysis. It also performs Zeta Potential measurements between -500 and +500 mV to analyze the stability of colloidal dispersions and estimate the charge of the adsorbent's surface [53].

2.2.4. Batch adsorption experiments

Heavy metal adsorption was carried out in a batch setup using 50 ml of solutions containing 10 mg/L of heavy metal solution at pH 7 which adjusted using 0.1 M HCl and 0.1 M NaOH solutions, shaken at a speed of 150 rpm at room temperature. The effect of various operational parameters such as contact time, temperature, initial concentration, pH, and dosage. The final concentrations were determined by the Agilent (ICP-MS) 7700. The Inductively Coupled Plasma Mass Spectrometry (ICP-MS 7700) is a cutting-edge analytical technique known for its high sensitivity and precision. This advanced form of mass spectrometry is capable of detecting both metals and nonmetals in materials at extremely low concentrations, even below one part per trillion [54]. The impact of mass on the adsorption process was studied by using 0.1, 0.2, and 0.3 grams of each adsorbent: chitosan, MOF, and MOF MIL (53) Fe/chitosan composite and shaking for 60 min. The impact of contact time on adsorption was investigated by using 0.3 g of adsorbent and shaking it for durations of 5, 20, 40, and 60 minutes. The effect of the starting concentration was investigated using 0.3 g adsorbent at three different concentrations: 0.1, 1, and 5 mg/L, with shaking for 60 minutes.

The Adsorption Capacity equation may be used to determine the quantity of adsorbed heavy metals on the adsorbent surface at any given time (t).

$$q_e = \frac{(C_0 - C_t)\, V}{m}$$

Where qe is the quantity of adsorbed heavy metals per unit mass of adsorbent (mg/g), C_o is the heavy metals' original concentration (mg/L), Ct is the equilibrium concentration (mg/L), V is the metals solution volume (L), and m is the mass of the composite (g).

The removal efficiency (Re) % is respectively calculated using the following equation [55, 56].

$$Re = \frac{(C0 - Ct))}{C0} \times 100$$

2.2.5. Adsorption isotherms

Different adsorption isotherms were utilized, such as Langmuir and Freundlich, to describe the adsorption equilibrium of the adsorbate onto the adsorbent. The Langmuir isotherm applies to monolayer chemisorption, while the Freundlich isotherm is used to describe adsorption on surfaces having heterogeneous energy distribution. The Freundlich linear equation is expressed as:

$$\log q_e = 1/n \log c_e + \log k_f$$

where (kf) (l/mg) and (1/n) Freundlich empirical constant is related to the total adsorption capacity of the solid.

The Langmuir equation is expressed as:

$$c_e / q_e = 1/k_L\, q_{max} + c_e/q_{max}$$

where qe (mg/g) is the heavy metal amount sorbed on the composite at equilibrium, qmax (mg/g) is the adsorption monolayer maximum capacity, kL is a constant related to the affinity between the adsorbate and the adsorbent, and it is related to the free energy of adsorption, and (Ce) (mg/l) is the concentration of heavy metals in the liquid phase at equilibrium [57,58].

3. Results and Discussion

3.1. Adsorbents characterization

The pore volumes, specific surface area, and pore sizes of the three adsorbents may be quantified using a BET apparatus at ambient air pressure and at the boiling point of liquid nitrogen, with a degassing temperature of 200°C [59-61]. The surface area for the three samples is reported in Table 1.

Table 1: The surface area of the three adsorbents

Adsorbent	**Surface area (m^2/g)**	**Surface area according to the latest methods and results (m^2/g)**	
Chitosan	(16.5)	Cu	(0.58 and 1.499) [62, 63]
		Cr	(7.876 to 492.133) [64]
		Zn	(28.141) [65]
		Pb	(12.3) [66]
MOF MIL (53) Fe	(3.5)	Cu	(71.93 and 194.41) [67, 68]
		Cr	
		Zn	
		Pb	
MOF MIL (53) Fe / Chitosan composite	(109.038)	Cu	(1.7973 and 27.7) [69, 70]
		Cr	
		Zn	
		Pb	

The surface area of an adsorbent plays a critical role in determining its adsorption capacity, as it directly influences the number of available active sites for contaminant binding. In this study, the BET surface areas of chitosan, MOF MIL(53) Fe, and the MOF MIL(53) Fe/chitosan composite were found to be 16.5 m^2/g, 3.5 m^2/g, and 109.038 m^2/g, respectively. The relatively low surface area of pristine MOF MIL(53) Fe may be attributed to its compact crystalline structure, which can limit pore accessibility. Interestingly, the composite exhibited a significantly higher surface area than either of the individual components, indicating a successful integration of the porous framework of the MOF with the biopolymeric network of chitosan. This enhancement can be ascribed to the synergistic interaction between the components, which may prevent aggregation and promote a more accessible pore structure. These findings are consistent with previously reported ranges in the literature. For instance, chitosan-based materials have demonstrated surface areas ranging from 0.58 to 28.141 m^2/g depending on the target metal ion and synthesis conditions [62–66], while MOF MIL(53) Fe showed reported values from 71.93 to 194.41 m^2/g in Cu(II) adsorption studies [67, 68]. The MOF/chitosan composite has also been reported to reach surface areas up to 27.7 m^2/g in Cu systems [69, 70], although the value of 109.038 m^2/g in the present work suggests improved structural optimization. This substantial increase in surface area highlights the potential of the composite for enhanced adsorption performance, particularly in the removal of heavy metals from aqueous solutions.

The crystallinity of the samples was assessed using wide-angle X-ray diffraction analysis utilizing an X Pert PRO XRD apparatus, as seen in Figures 4, 5, and 6. The XRD charts of the chitosan adsorbent exhibit stronger peaks, indicating enhanced crystallinity. The existence of chitosan was identified from the peaks angle at (2θ) = (20°) with highest intensity at (110.54) count, (2θ) = (8.7°) with intensity at (58.96) count, (2θ) = (43.76°) at (13.74) count and (2θ) = (72.29°) with intensity at (58.88) count, all these angels are the fingerprint of chitosan [71,72]. The appearance of MOF was identified from the peak angles at (2θ) = (8.8°, 9.3°, 12.46°, 17.63°, 19.7°, 21.6°, and 26.59°) with high intensities at (237.59, 162.54, 26.31, 108.07, 20.46, 38.63, and 35.57) [73], the XRD patterns of chitosan/MOF composite adsorbent was identified from the peaks angle at (2θ) = (7°, 17°,21°,25°and 37°) with intensities at (51,23,17,14 and 11) [74]. the presence of peak angle at (2) theta with its high intensities is evidence of successful manufacturing of chitosan, MOF, and chitosan MOF composite.

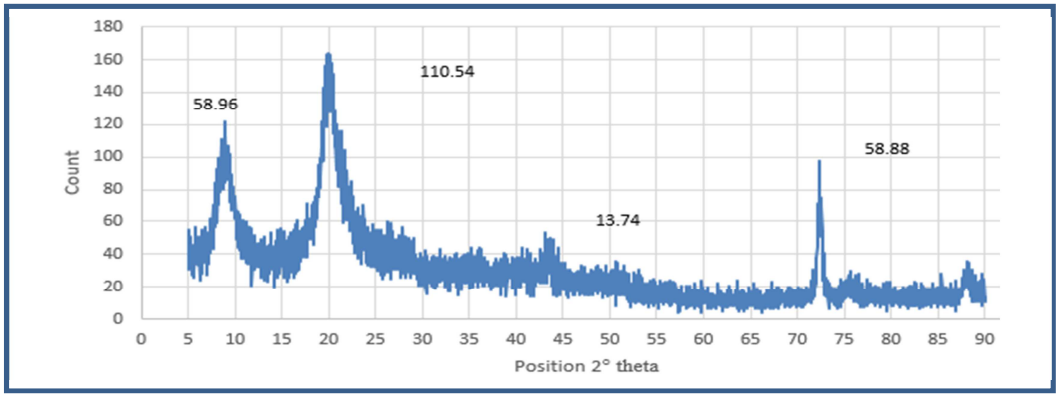

Fig. 4. XRD spectra of chitosan.

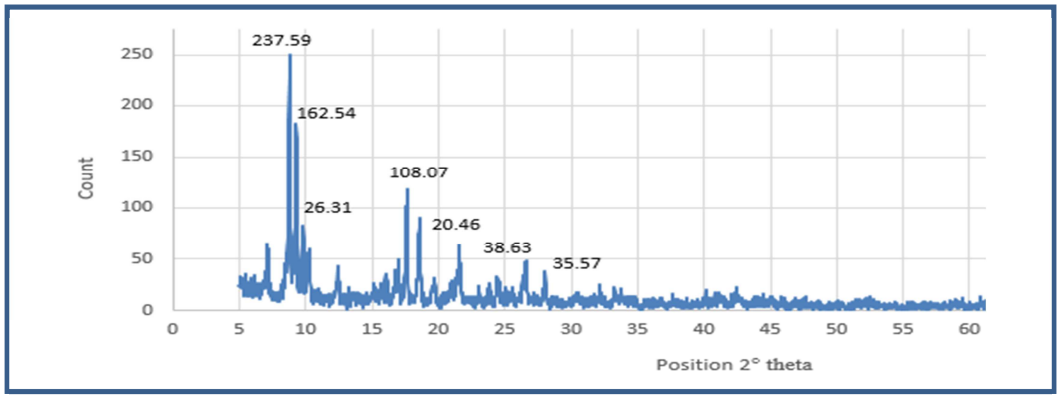

Fig. 5. XRD spectra of MOF.

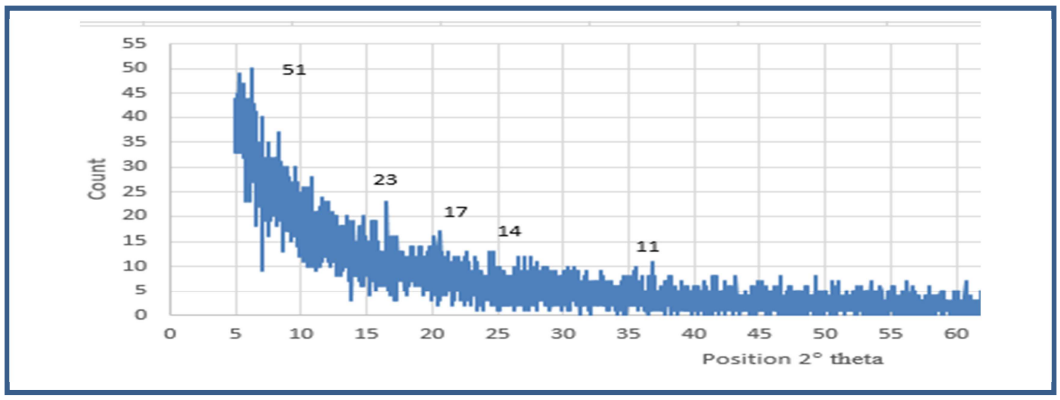

Fig. 6. XRD spectra of chitosan / MOF composite.

The Scanning Electron Microscope (SEM) was utilized to examine the morphological alterations and structural distinctions among Chitosan, MOF, and the chitosan/MOF composite, as illustrated in Figures 7, 8, and 9. The SEM images of chitosan showed a porous crystalline structure with particle aggregation of various sizes as a heterogeneous surface morphology. The average size of chitosan particles was observed from (500 to 20) µm, and the EDX analysis seen in Figure 10 showed that the weight percentage of (C) was (53.05)% and for (O) was (46.95)% [75]. The SEM images of MOF showed tiny different sizes of MOF particles that were observed from (50 to 10) µm, and the EDX analysis showed that the weight percentage of (C) was

(49.53)%, for (O) was (34.9)%, for (Cl) was (2.77)%, and for (Fe) was (12.98)% [76]. The SEM images of MOF-chitosan showed a heterogeneous surface of various sizes with the average size of MOF-chitosan particles ranging from 500 to 20 µm. The EDX analysis showed that the weight percentage of (C) was (24.89%), (O) was (51.59%), (Na) was (13.37%), and (P) was (10.15%). Table 2 illustrates a summary of EDX results.

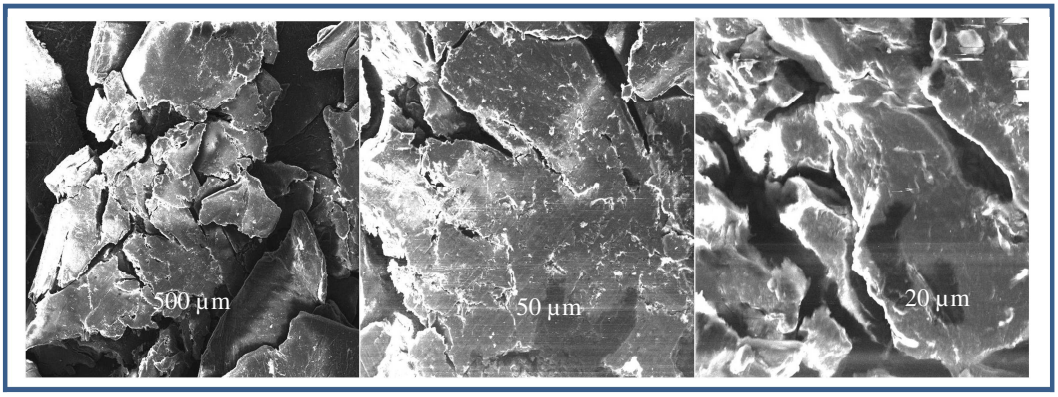

Fig. 7. SEM images of chitosan.

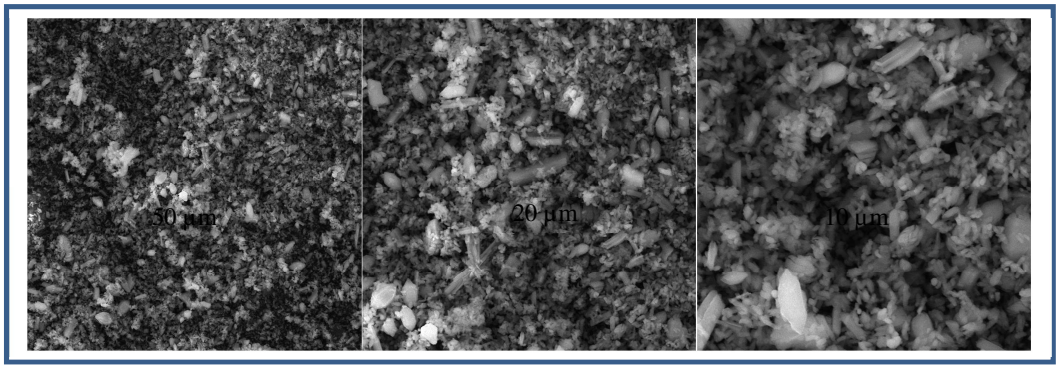

Fig. 8. SEM images of MOF.

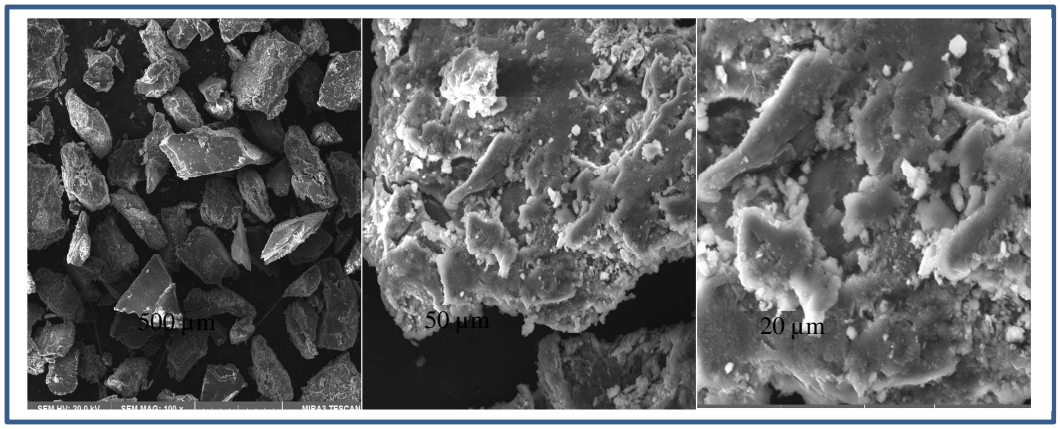

Fig. 9. SEM images of Chitosan / MOF composite.

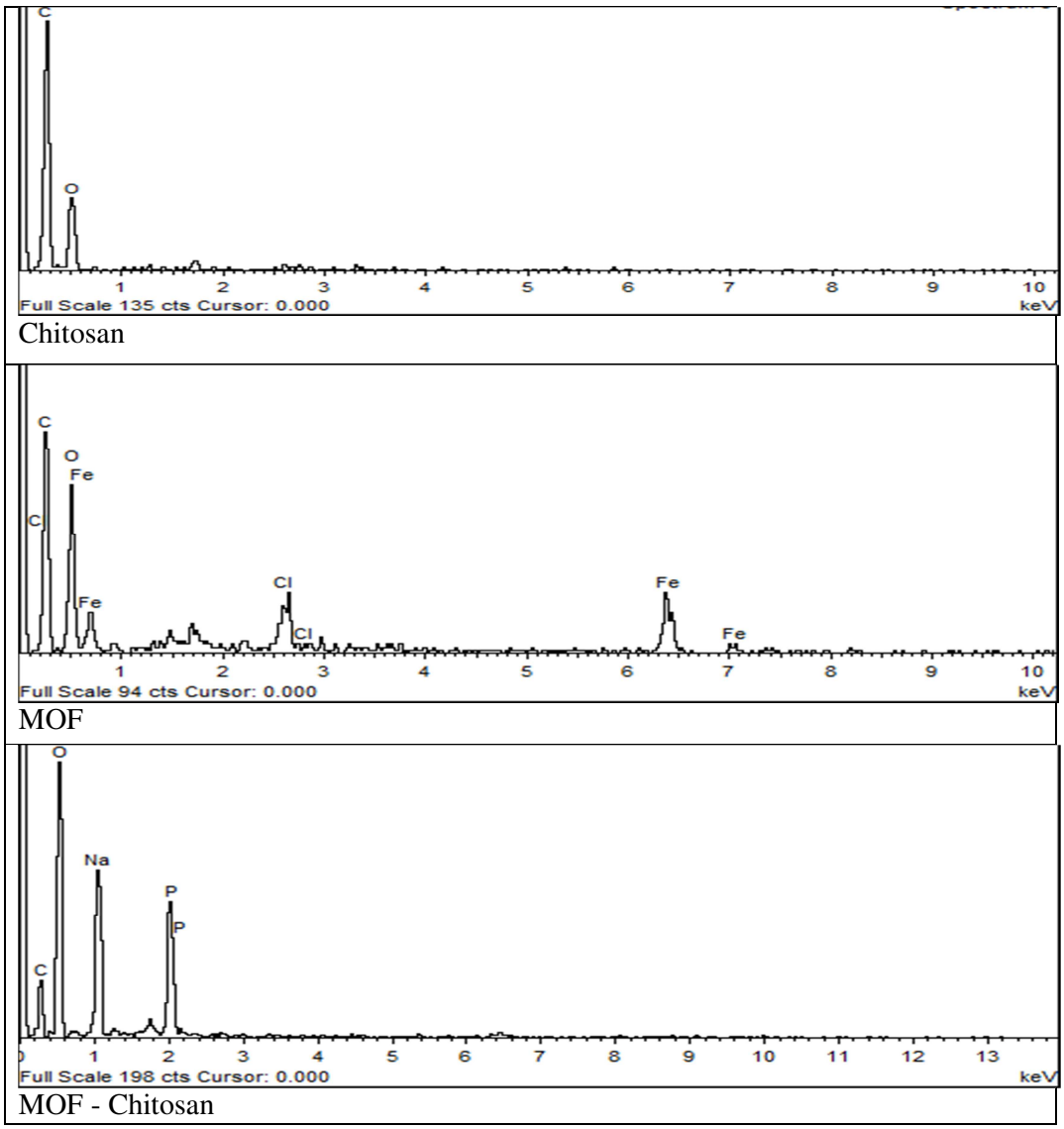

Fig. 10. Spectrum of chitosan, MOF and chitosan / MOF composite.

Table 2: The EDX analysis of chitosan, MOF, and chitosan/MOF composite.

Element (Wt. %)	C	O	Cl	Fe	Na	P
Chitosan	53.05	46.95	___	___	___	___
MOF	49.53	34.9	2.77	12.98	___	___
Chitosan / MOF composite	24.89	51.59	___	___	13.37	10.15

The FTIR spectra were recorded in the range of 500 to 4000 cm^{-1}, as illustrated in Figures 11, 12, and 13. These spectra demonstrate an abundance of functional groups, including carbon, nitrogen, and oxygen. The spectrum shows that the distinctive peaks of chitosan are consistent with those described in other investigations. A significant spectrum between 500 and 3291 cm^{-1} correlates to N-H and O-H stretching, in addition to intramolecular hydrogen bonding. Absorption bands near 2921 and 2872.32 cm^{-1} are associated with C-H stretching, which is in agreement with the spectra of polysaccharides such as Xylan. The existence of residual N-acetyl groups was confirmed by the bands at (1652.73) cm^{-1} (C=O stretching of amide I) and (1312.5) cm^{-1} (C-N stretching of amide III). A small band at (1540.34) cm^{-1} corresponds to N-H bending of amide II, a band at (1586.38) cm^{-1} corresponds to the N-H bending of the primary amine, and the CH_2 bending and CH_3 were confirmed by the existence of bands at around (1423.52) and (1374.45) cm^{-1}. The absorption band at (1149.91) cm^{-1} corresponds to the C-O-C bridge. The bands at (1065.210 and (1026.73) cm^{-1} correspond to C-O stretching. The signal at (894.73) cm^{-1}

corresponds to the CH bending out of the plane of the ring of monosaccharides. The broad band at (3600 to 4000) cm^{-1} indicates the existence of adsorbed water on the material. The presence of all transmittance peaks indicates the successful synthesis of chitosan [77]. The spectrum of MOF MIL (53) Fe shows the Fe-O bond between the carboxylic group of the ligand and Fe (III) was observed at (527.73) cm^{-1}. C–H bending vibration of benzene rings of the linker is a sharp peak that was observed at (732.03) cm^{-1}. The broad bands at (1387.03 and 1509.49) cm^{-1} were stretching vibrations of C–O bonds in the carboxylic group. The peak at (1678.82) cm^{-1} can be annotated to the C=O stretching the carboxylic group [78, 79]. The FTIR spectrum of chitosan/MOF shows absorbance peaks at (2872.32, 1558.55, 1374.34, 1031.49, and 514.62) cm^{-1}, which correspond to C–H, N–H, C–H, C–O, and Fe–O bonds, respectively. The FTIR spectrum of the Chitosan/MOF MIL-53(Fe) composite displays typical peaks with less intensity and a shift toward greater wave numbers, showing that Fe ions were successfully incorporated into the composite. Peaks at 1631.3 and 1692.5 cm^{-1} indicate the creation of coordination bonds between carboxylic groups and the Fe metal ion. The low strength of these peaks verifies the composite's homogeneity [80].

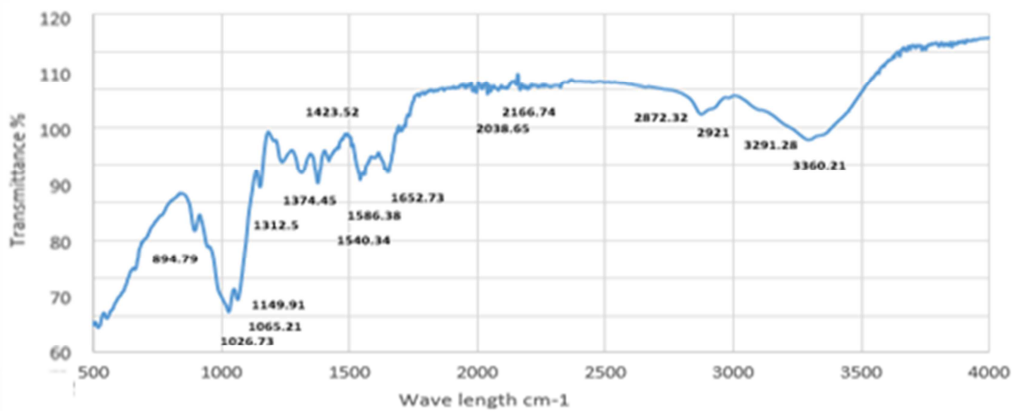

Fig. 11. FTIR spectra of Chitosan.

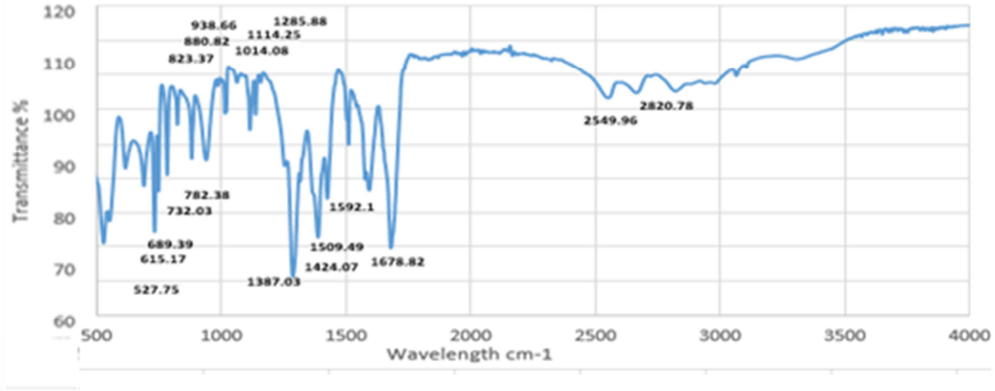

Fig. 12. FTIR spectra of MOF.

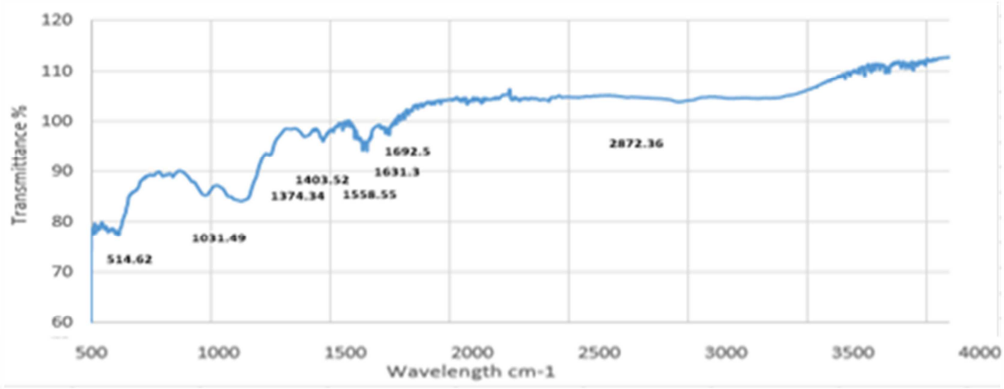

Fig. 13. FTIR spectra of Chitosan / MOF composite.

For Raman spectrum analysis of chitosan, a succession of linked signals may be detected in the range (500-4500) cm^{-1} [81], as shown in Figures 14, 15, and 16. The peaks can be annotated as CH stretching vibration at (2877) cm^{-1}. The CO amide (I) stretching vibration at (1626) cm^{-1}. The NH amide (II) stretching vibration at (1588.5) cm^{-1}, amide (III) at (1359) cm^{-1}, and the CC stretching region (1005.5-1186) cm^{-1}. The CNH bending region (1203) cm^{-1}. G peak is higher than D peak, which means that all carbons are sp3, the ID/IG = 0.5771 [82, 83]. For MOF MIL (53), Fe signals C-H bonds at (620, 871) cm^{-1} and C-C bonds at (1147.5) cm^{-1} of benzene rings. O-C-O bonds at (1432.5, 1492.5) cm^{-1} of acid groups that support the structural consolidation of MOF MIL-53 (Fe) [84]. The presence of O-H groups on the MOF surface caused a wide band of about (3200-3600) cm^{-1} due to water adsorption. C-O stretching of dicarboxylate linkers may be verified as sharp vibrations at (1422) cm^{-1}, carboxylate ligand (C=O) was visible at (1608) cm^{-1}, and C-H at (858) cm^{-1} that belongs to the carboxylate's aromatic rings. Coordination bonds between (Fe) III and -OOC-C6H4-COO- carboxylate anions were found at a low wavenumber of 436.5 cm^{-1}.

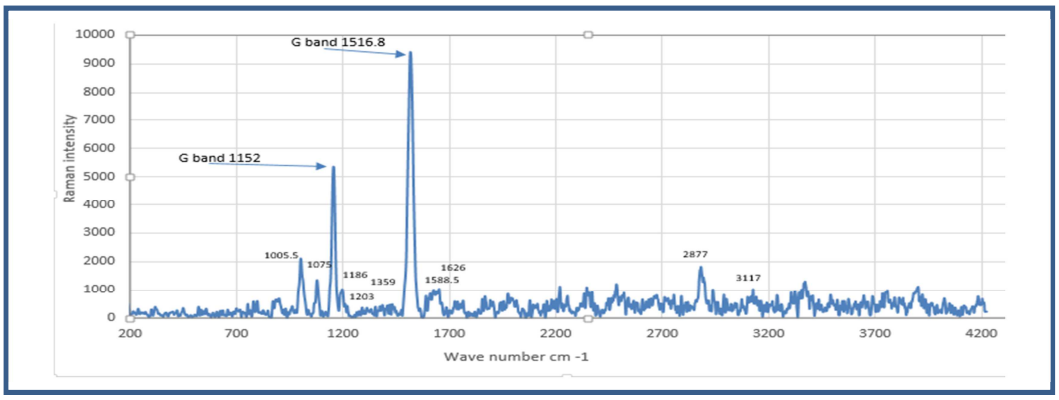

Fig. 14. Raman Spectra of Chitosan.

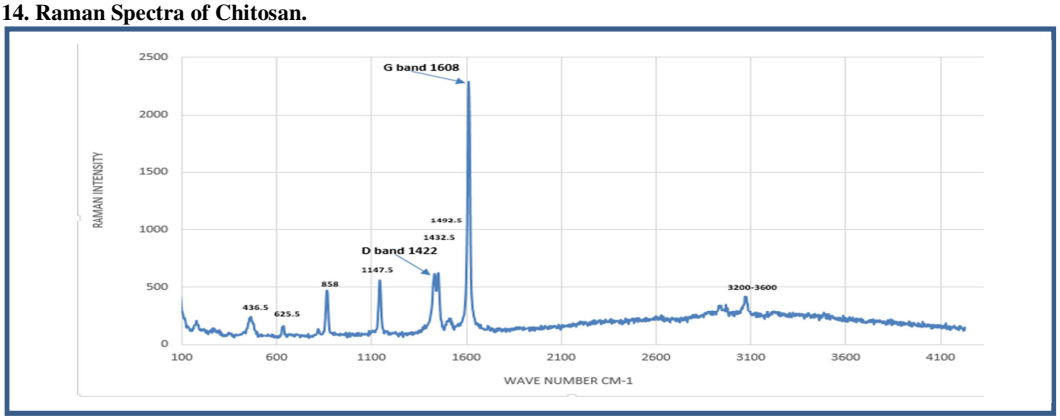

Fig. 15. Raman Spectra of MOF.

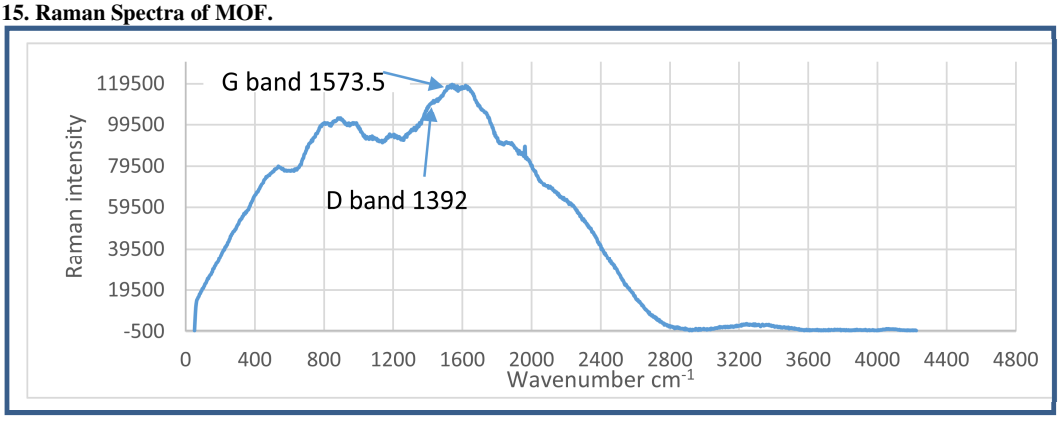

Fig. 16. Raman Spectra of Chitosan/MOF composite.

The presence of a Fe-O bond in the structure of MOF MIL (53) Fe indicates that the crystals of MOF MIL were effectively produced. G peak is higher than D peak, which means that all carbons are sp3, the ID/IG = 0.2605 [85, 86]. MOF/Chitosan composite peaks are the D band at (1392) cm^{-1} and the G band at (1573.5) cm^{-1}. These two bands confirm that the composite was successfully synthesized. If carbon material is fully oxidized, that means all carbons are sp3, but if the D peak is higher than the G peak, the sp2 bonds are broken, which means that there are more sp3 bonds and more transition from sp2 to sp3 material. In our composite, the G peak is greater than the D peak, indicating that all carbons are sp^3, with ID/IG = 0.9148 [87].

The shape and size of the three adsorbents were investigated using an F200I transmission electron microscope (TEM), as illustrated in Figures 17-19. TEM was utilized to examine the morphological alterations and structural differences between chitosan, MOF, and chitosan/MOF composite. A TEM micrograph of chitosan revealed a smooth enamel surface with a regular pattern, as well as excellent and random dispersion of the chitosan matrix. It discovered a porous crystalline structure with particle aggregation of varying sizes as a heterogeneous surface appearance. The typical chitosan size ranged from 50 to 1000 nm. The MOF TEM pictures were extremely clear; they showed a good shape of conical particles, indicating a variety of MOF particle sizes collected together, resulting in the successful production of the MOF MIL 53 (Fe). The mean size of MOF particles ranged between 50 and 1000 nm. The MOF MIL 53(Fe) crystals exhibit a consistent size distribution, as do the particles [88]. The TEM images of the chitosan/MOF composite showed excellent aggregation between chitosan particles and conical particles of MOF, forming a homogenous layer of cross-linked crystals with various sizes as a heterogeneous surface morphology, which gives excellent evidence about the successful fabrication process of the composite. The mean size of the chitosan/MOF composite ranged from 20 to 500 nm.

Figures 20, 21, and 22 show that the zeta potential of chitosan was -27.5 mV, that of MOF was +37.8 mV, and that of the chitosan/MOF composite was -42.8 mV. A zeta potential value of more than +30 mV or less than -30 mV is often regarded as indicative of excellent vesicle stability. A positive zeta potential implies that the dispersed particles in the suspension are positively charged, whereas a negative zeta potential indicates negatively charged particles. Zeta potential values ranging from 30 to 60 mV in absolute terms are regarded as good to excellent stability, which was observed for all three adsorbents [89-91].

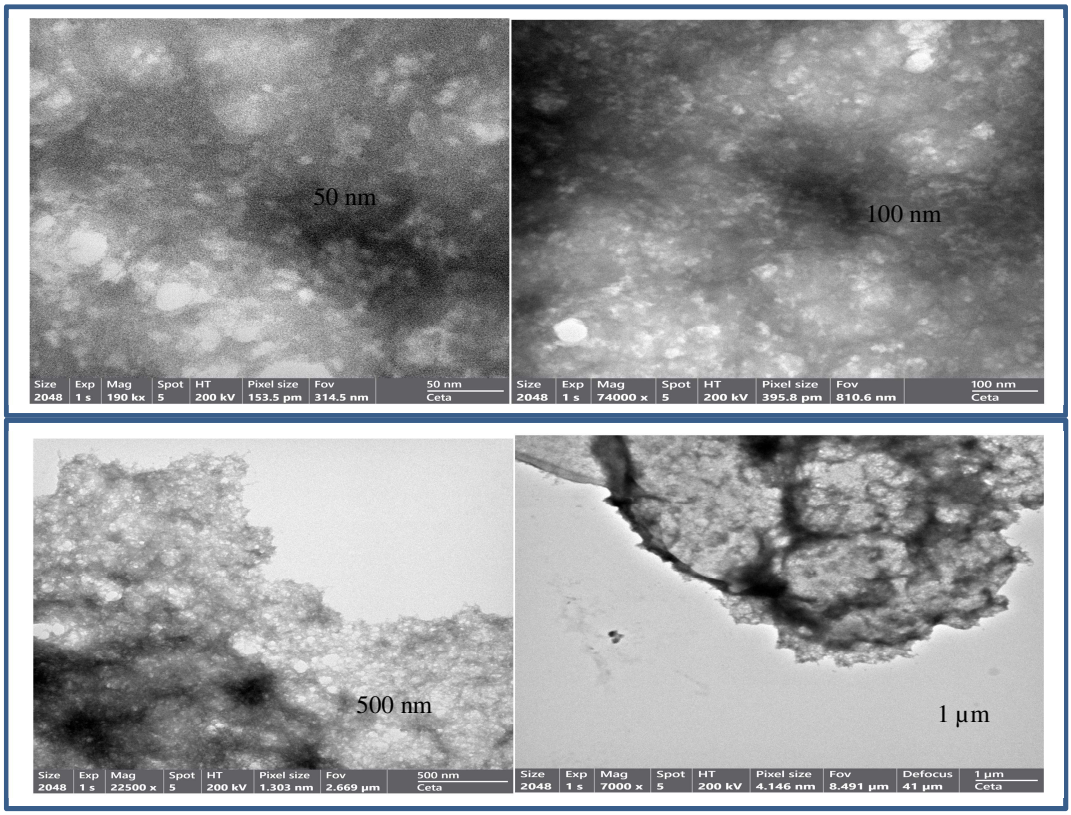

Figure 17. TEM image of chitosan.

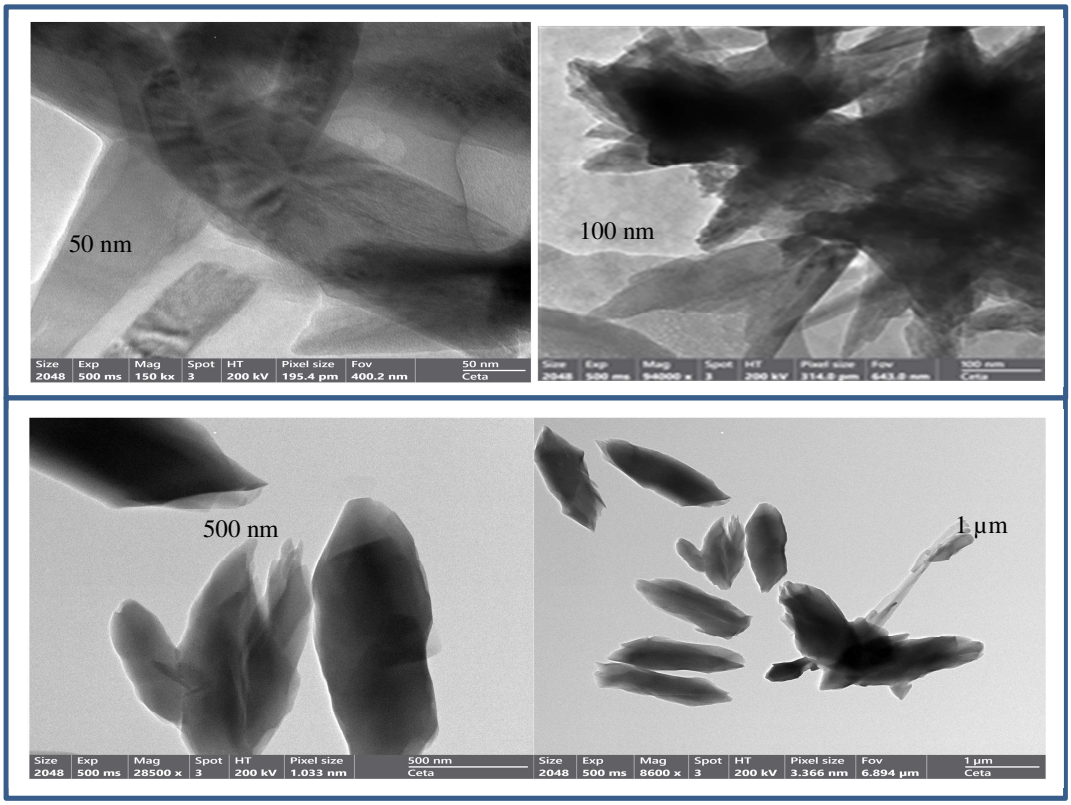

Figure 18. TEM image of MOF.

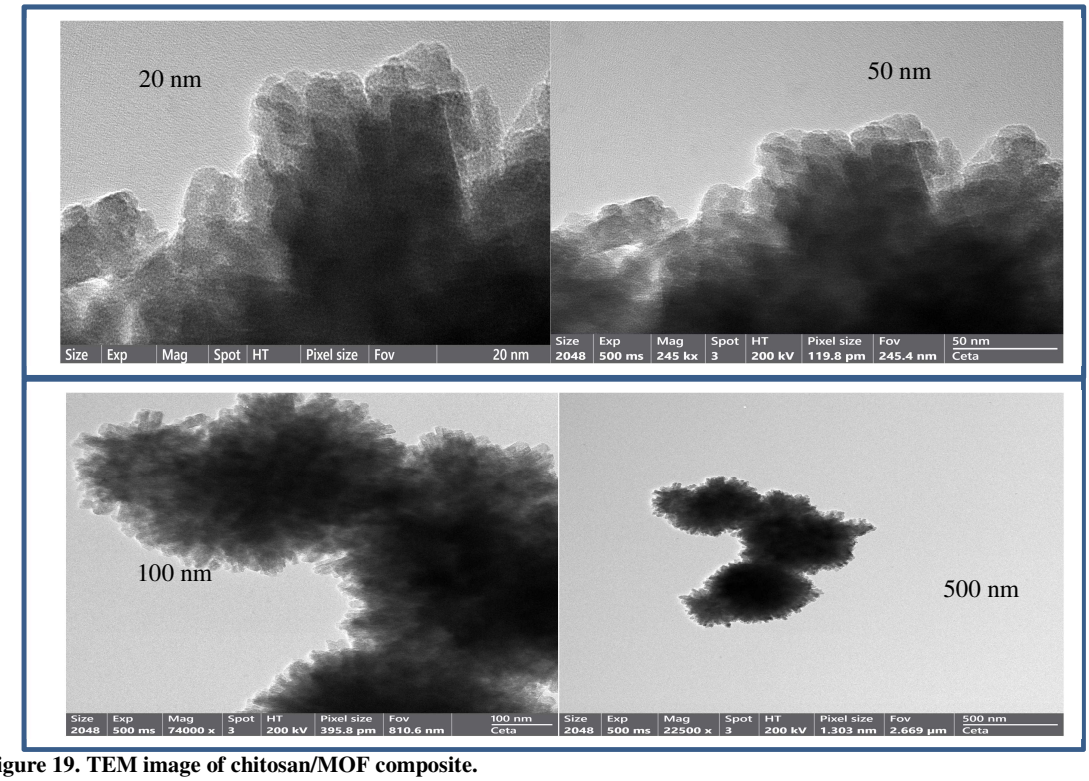

Figure 19. TEM image of chitosan/MOF composite.

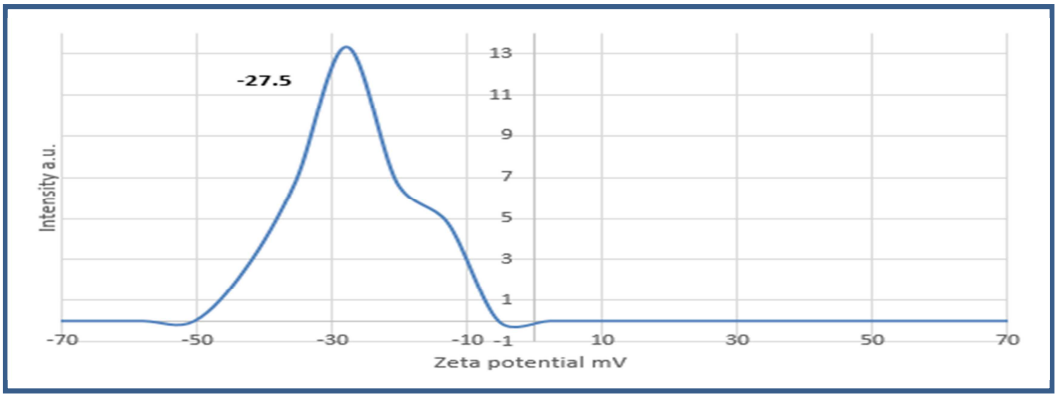

Figure 20. Zeta potential of chitosan.

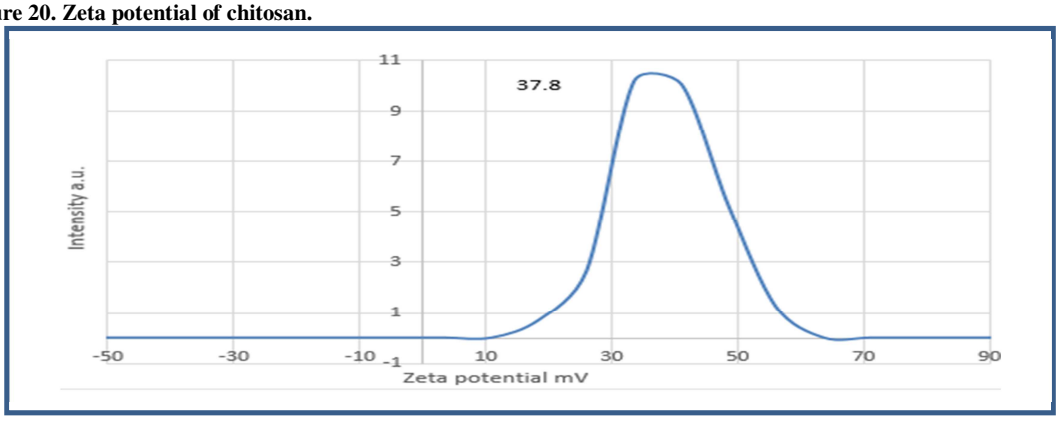

Fig. 21. Zeta potential mean of MOF.

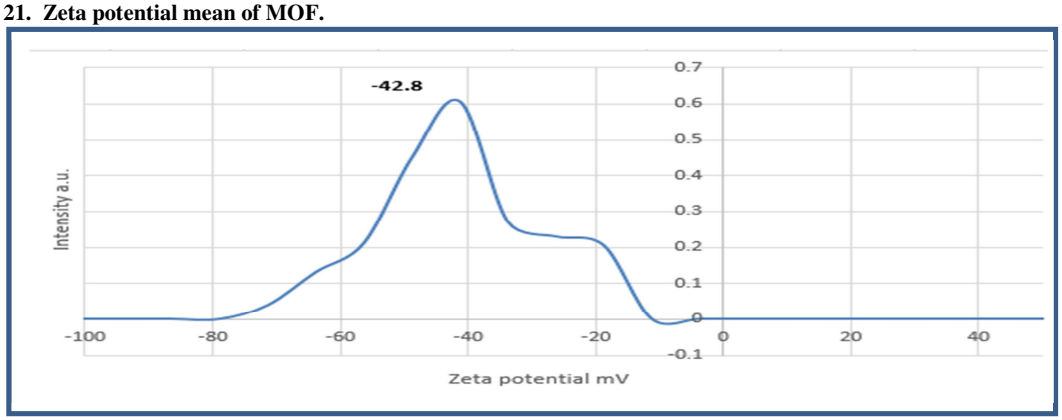

Fig. 22. Zeta potential mean of Chitosan/MOF composite.

3.2. Sorption experiments

3.2.1. Effect of solution pH

The solution pH has a major effect on chitosan solubility and electrical charges. Chitosan is soluble in inorganic acids at ambient temperature with a pH less than 6. During this investigation, chitosan was tested at pH levels of 4, 7, and 10. The maximum removal efficiencies observed were 92.2% for Cu, 90.8% for Cr, 82.2% for Zn, and 91.2% for Pb. The highest removal efficiency for copper, chromium, zinc, and lead occurred at pH 7. Additionally, the maximum adsorption capacities were 2.3 mg/g for Cu, 2.27 mg/g for Cr, 2.05 mg/g for Zn, and 2.28 mg/g for Pb. Again, pH 7 had the best sorption capacity and removal efficiency for all four metals. MOF (Metal-Organic Framework) is generally recognized as an iron carboxylate framework with notable stability in water. The influence of pH on the stability of MOF in water was studied at pH values 4, 7, and 10. The highest removal efficiencies were recorded for Cu (99.58%), Cr (99.76%), Zn (99.8%), and Pb (99.6%). The

greatest sorption capacities for Cu were 2.48 mg/g, Cr 2.494 mg/g, Zn 2.495 mg/g, and Pb 2.49 mg/g. Similar to chitosan, pH 7 has the maximum sorption capacity for chromium, copper, zinc, and lead. At pH values of 4, 7, and 10, the Chitosan/MOF MIL-53(Fe) combination achieved the highest removal efficiency of 94.95% for Cu, 93.4% for Cr, 88.62% for Zn, and 94.31% for Pb. The greatest sorption capacities were 2.37 mg/g for Cu, 2.33 mg/g for Cr, 2.21 mg/g for Zn, and 2.35 mg/g for lead. Once again, pH 7 demonstrated the best sorption capacity for chromium, copper, zinc, and lead [92] as seen in Figures 23 and 24.

3.2.2. Effect of adsorbent doses

To investigate the effect of adsorbent dosages, we employed three different adsorbent doses (0.1, 0.2, and 0.3 grams). The greatest Cu removal efficiency was 99.48%, Cr 96.2%, Zn 99.54%, and 99.9% for Pb. The maximum removal efficiency for copper, chromium, zinc, and lead was attained with a 0.3 mg adsorbent dosage. Cu had the highest sorption capacity of 2.472 mg/g, followed by Cr at 2.34 mg/g, Zn at 2.479 mg/g, and Pb at 2.43 mg/g. 0.3 mg adsorbent dosage achieved the maximum sorption capacity for copper, chromium, zinc, and lead, respectively [94]. The greatest Cu removal efficiency for MOF was 85.4%, Cr 99.6%, Zn 93%, and 99.8% for Pb. The greatest sorption capacity of Cu was 1.95 mg/g, Cr 2.475 mg/g, Zn 2.185 mg/g, and 2.48 mg/g for Pb. The sorbent dosage at (0.3) had the best removal efficiency and sorption capacity for copper, chromium, zinc, and lead, respectively [95]. Using Chitosan/MOF MIL (53) Fe composite, the greatest removal efficiency of Cu was 98.4%, Cr 98.6%, Zn 96.2%, and 99.8% for Pb. The greatest sorption capacity for Cu was 2.345 mg/g, Cr 2.375 mg/g, Zn 2.325 mg/g, and 2.46 mg/g for Pb. The sorbent dosage of 0.3 resulted in the best removal efficiency and sorption capacity for copper, chromium, zinc, and lead, as shown in Figures 25 and 26.

3.2.3. Effect of concentration

Using various heavy metal concentrations of 0.1, 1, and 5 ppm, the greatest removal efficiency was 99.47% for Cu, 99.62% for Cr, 99.52% for Zn, and 99.97% for Pb. The greatest sorption capacity was 0.828 mg/g for Cu, 0.83 mg/g for Cr, 0.829 mg/g for Zn, and 0.833 mg/g for Pb. The metal at 5 ppm resulted in the maximum elimination efficiency and sorption capacity for copper, chromium, zinc, and lead, respectively. For MOF, the greatest removal efficiency was 80.74% for Cu, 99.22% for Cr, 82.6% for Zn, and 99.48% for Pb. The greatest sorption capacity was 0.672 mg/g of Cu, 0.826 mg/g for Cr, 0.688 mg/g for Zn, and 0.829 mg/g for Pb. The concentration of 5 ppm had the maximum removal efficiency and sorption capacity for copper, chromium, zinc, and lead. Using the Chitosan/MOF MIL (53) Fe composite at various concentrations, the greatest removal efficiency was 96.4% of Cu, 97.04% for Cr, 94.52% for Zn, and 99.78% for Pb. The greatest sorption capacity was 0.803 mg/g for Cu, 0.808 mg/g for Cr, 0.787 mg/g for Zn, and 0.931 mg/g for Pb. The concentration of 5 ppm had the maximum removal efficiency and sorption capacity for copper, chromium, zinc, and lead, as seen in Figures 27 and 28.

3.2.4. Effect of contact time

At varying contact durations of 5, 20, 40, and 60 minutes, the greatest removal efficiencies were 97% for copper, 97.6% for chromium, 96.8% for zinc, and 98% for lead. The greatest sorption capacities were 0.808 mg/g for Cu, 0.813 mg/g for Cr, 0.806 mg/g for Zn, and 0.816 mg/g for Pb. The contact duration of 60 minutes yielded the best removal efficiency and sorption capacity for copper, chromium, zinc, and lead, respectively. The greatest removal efficiencies of Cu, Cr, Zn, and Pb for MOF were 97.98%, 97.62%, 95.8%, and 98.4%, respectively. The greatest adsorption capacity was 0.816 mg/g for Cu, 0.8135 mg/g for Cr, 0.798 mg/g for Zn, and 0.82 mg/g for Pb. The contact period of 60 minutes resulted in the maximum removal efficiency and sorption capacity for copper, chromium, zinc, and lead. Using Chitosan/MOF MIL (53) Fe composite at various concentrations, the greatest Cu removal effectiveness was 98.4%, 97.8% for Cr, 96.8% for Zn, and 99.58% for Pb. The greatest sorption capacity of Cu was 0.82 mg/g, 0.815 mg/g for Cr, 0.806 mg/g for Zn, and 0.829 mg/g for Pb. The contact period of 60 minutes resulted in the maximum removal efficiency and sorption capacity for copper, chromium, zinc, and lead (see Figures 29 and 30).

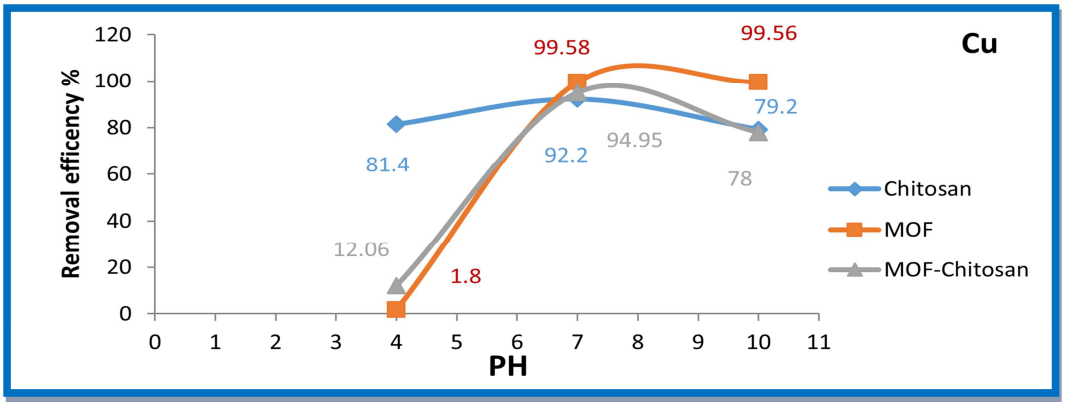

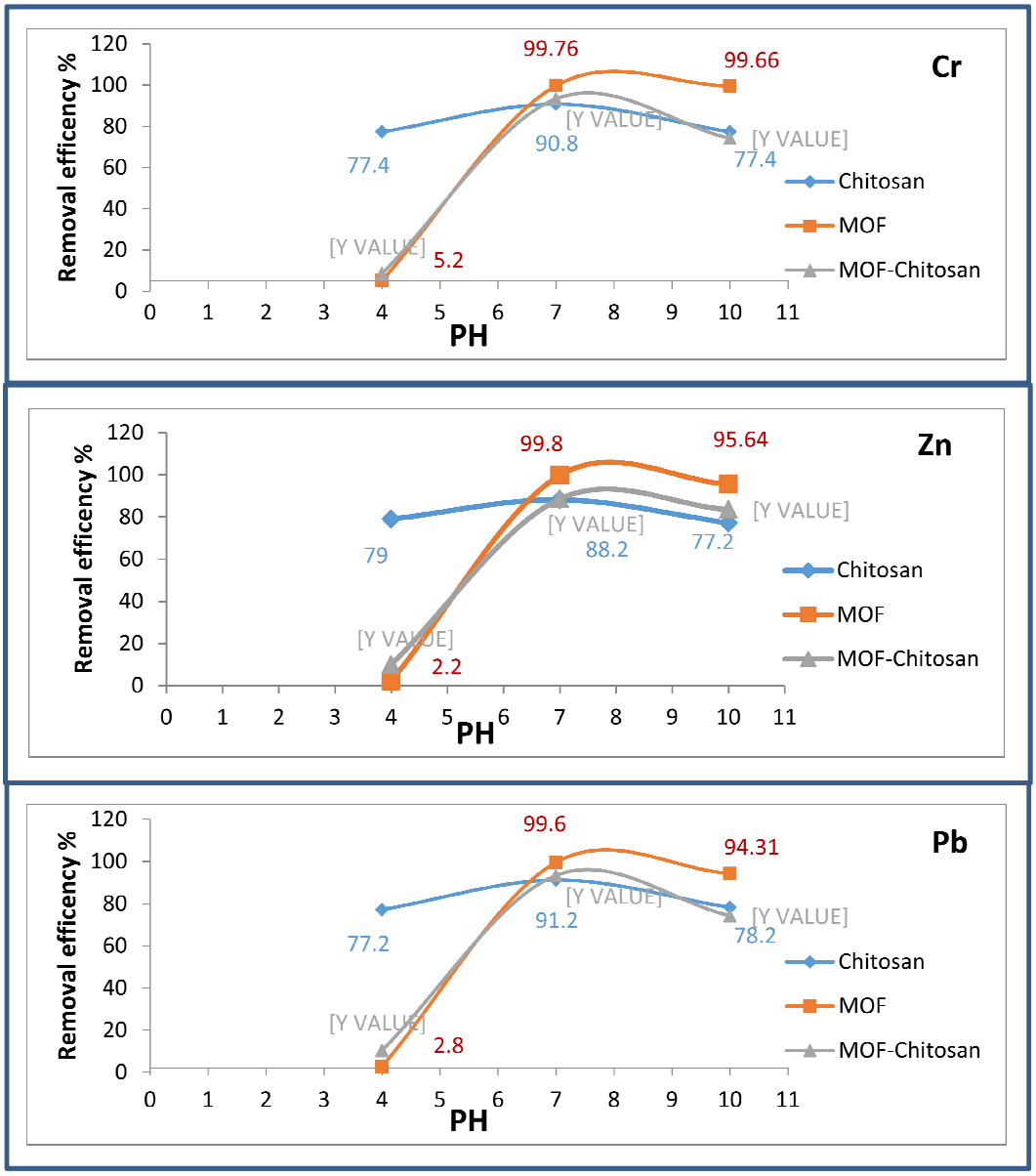

Fig. 23. Effect of pH on removal efficiency.

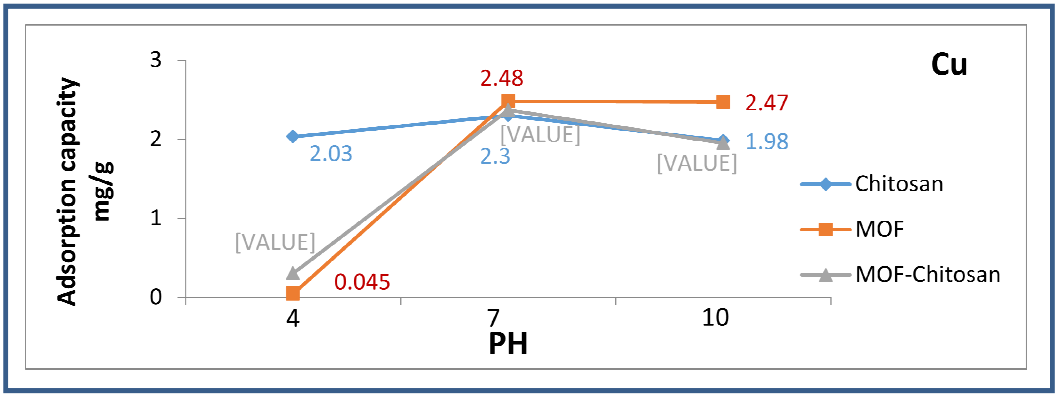

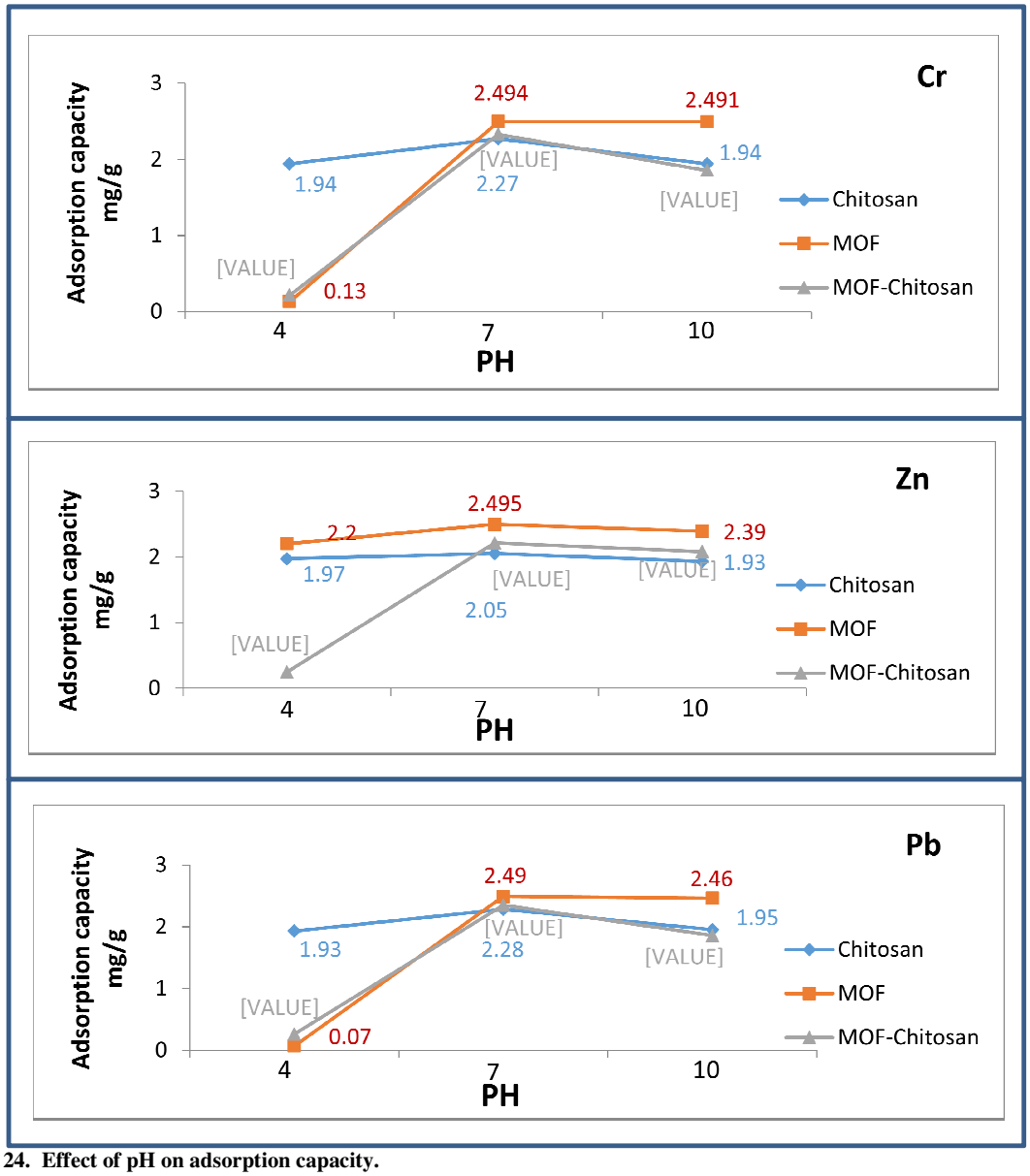

Fig. 24. Effect of pH on adsorption capacity.

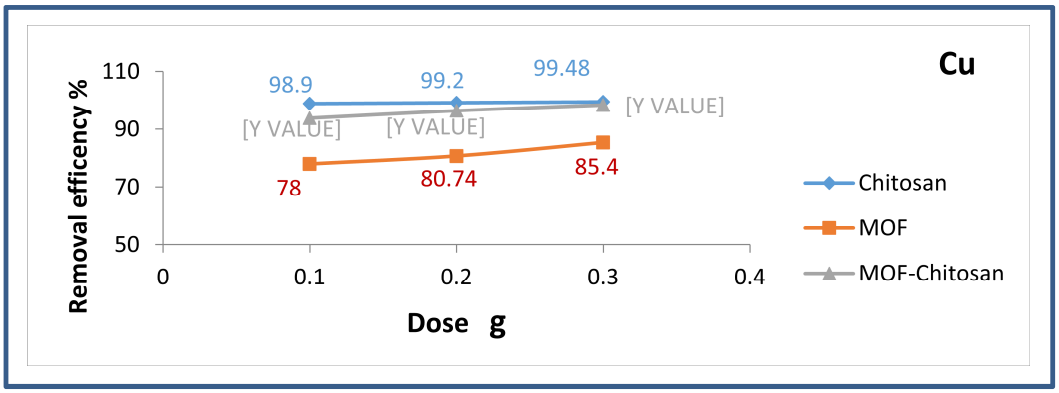

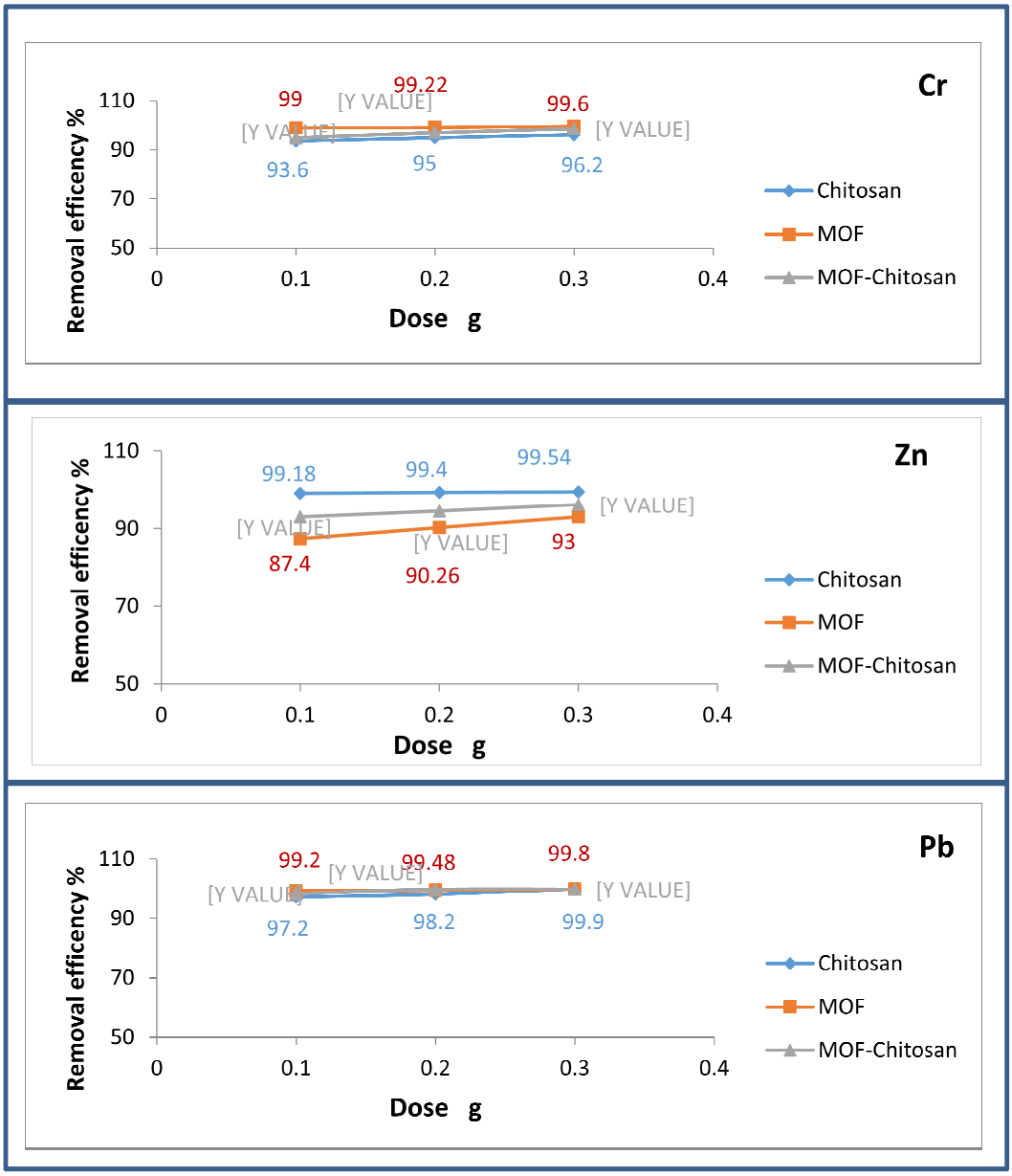

Fig. 25. Effect of adsorbent doses on removal efficiency.

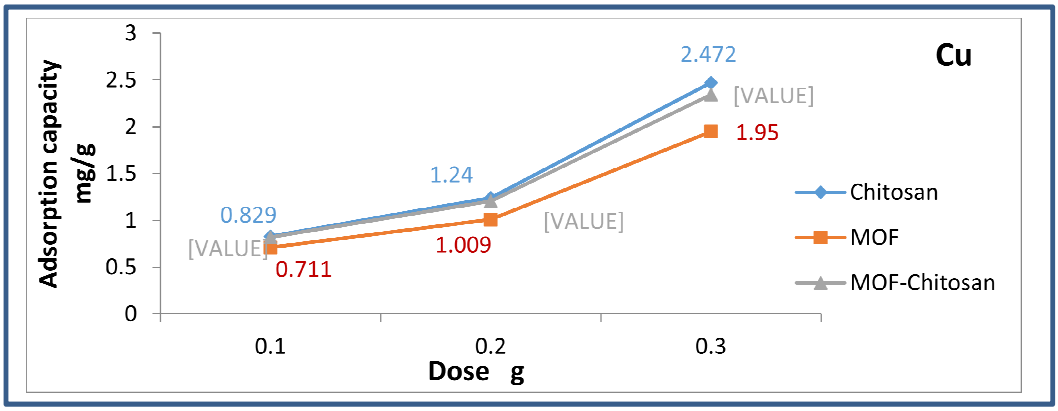

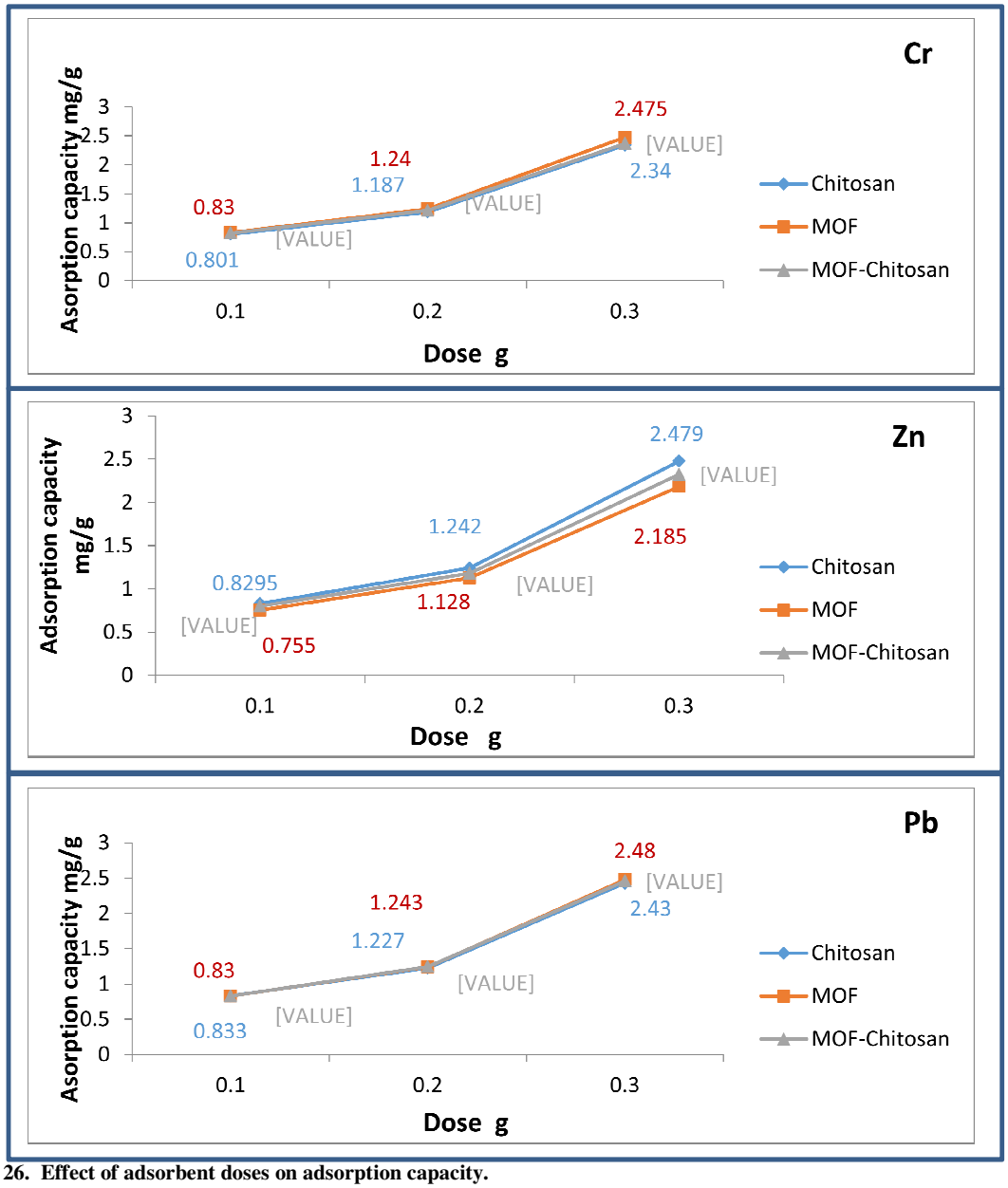

Fig. 26. Effect of adsorbent doses on adsorption capacity.

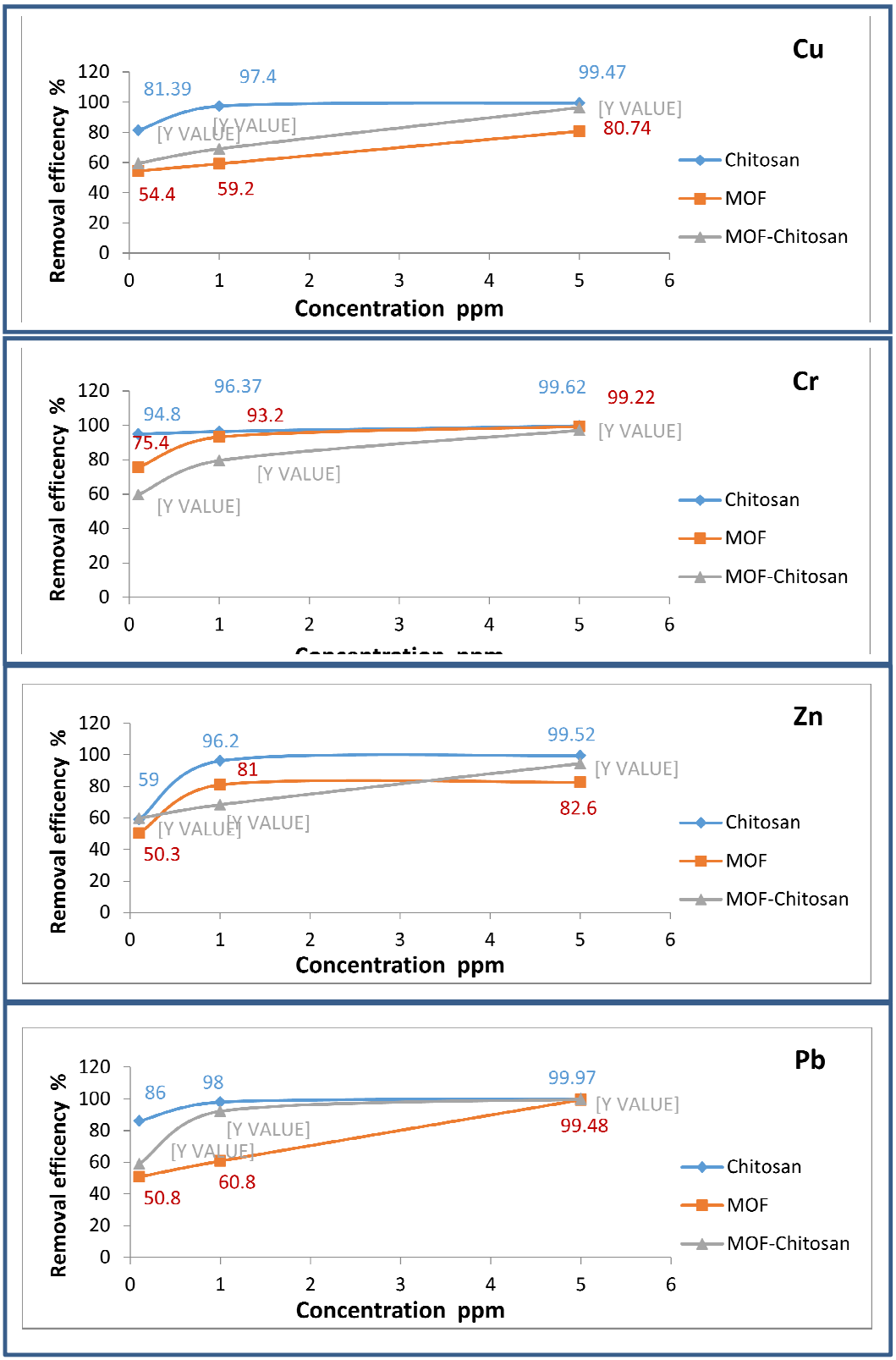

Fig. 27. Effect of concentration on removal efficiency.

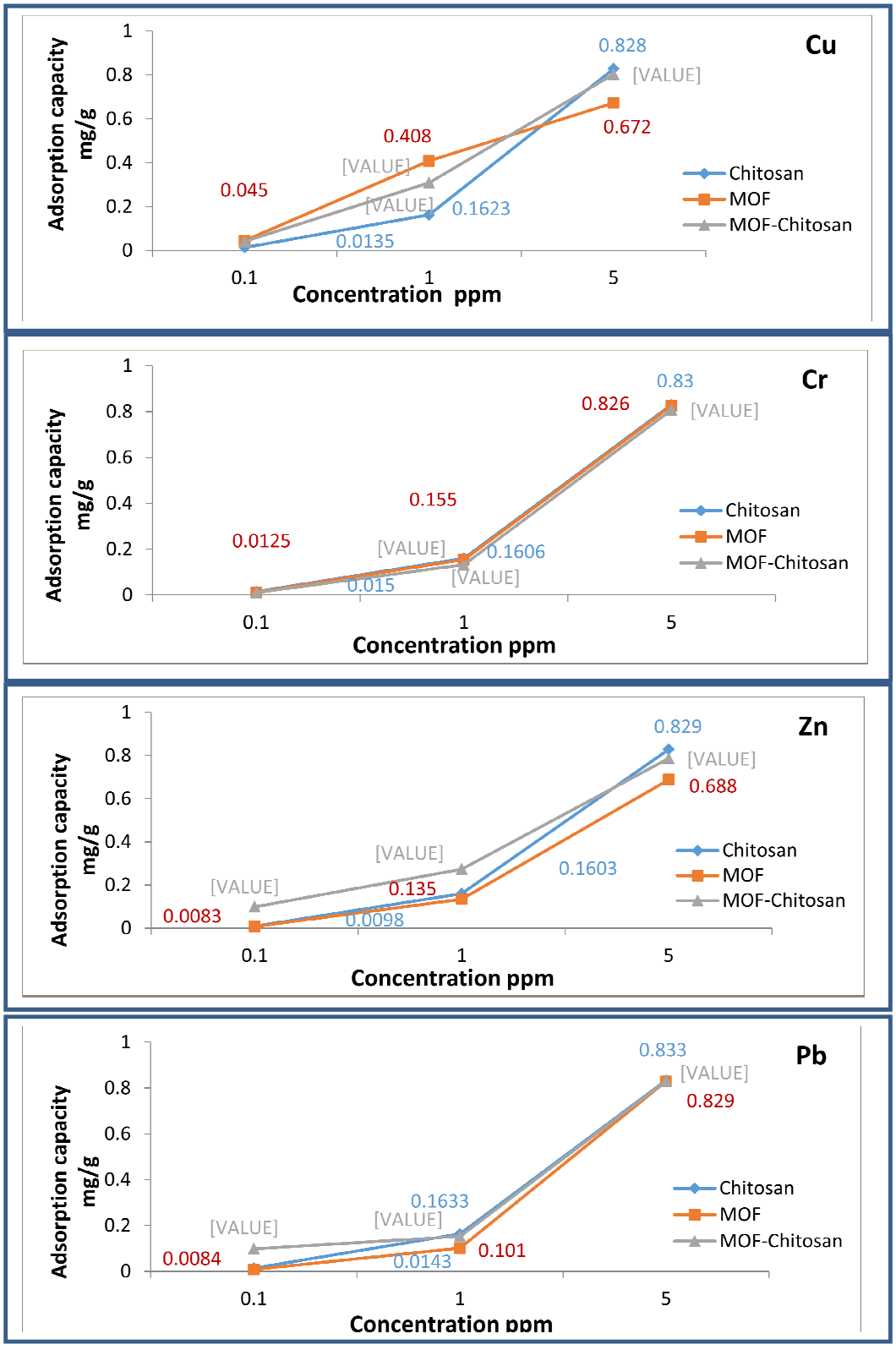

Fig. 28. Effect of concentration on adsorption capacity.

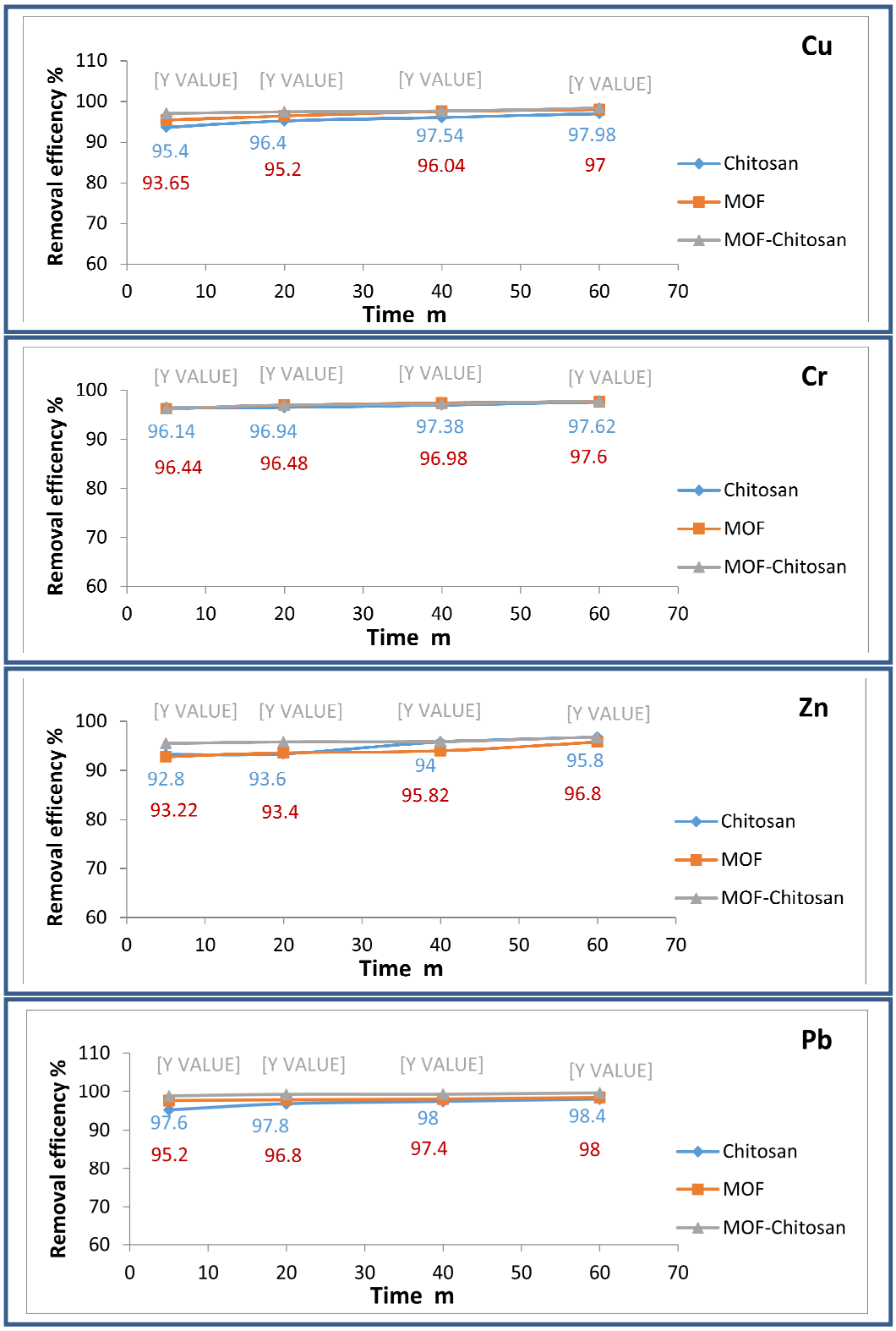

Fig. 29. Effect of contact time on removal efficiency.

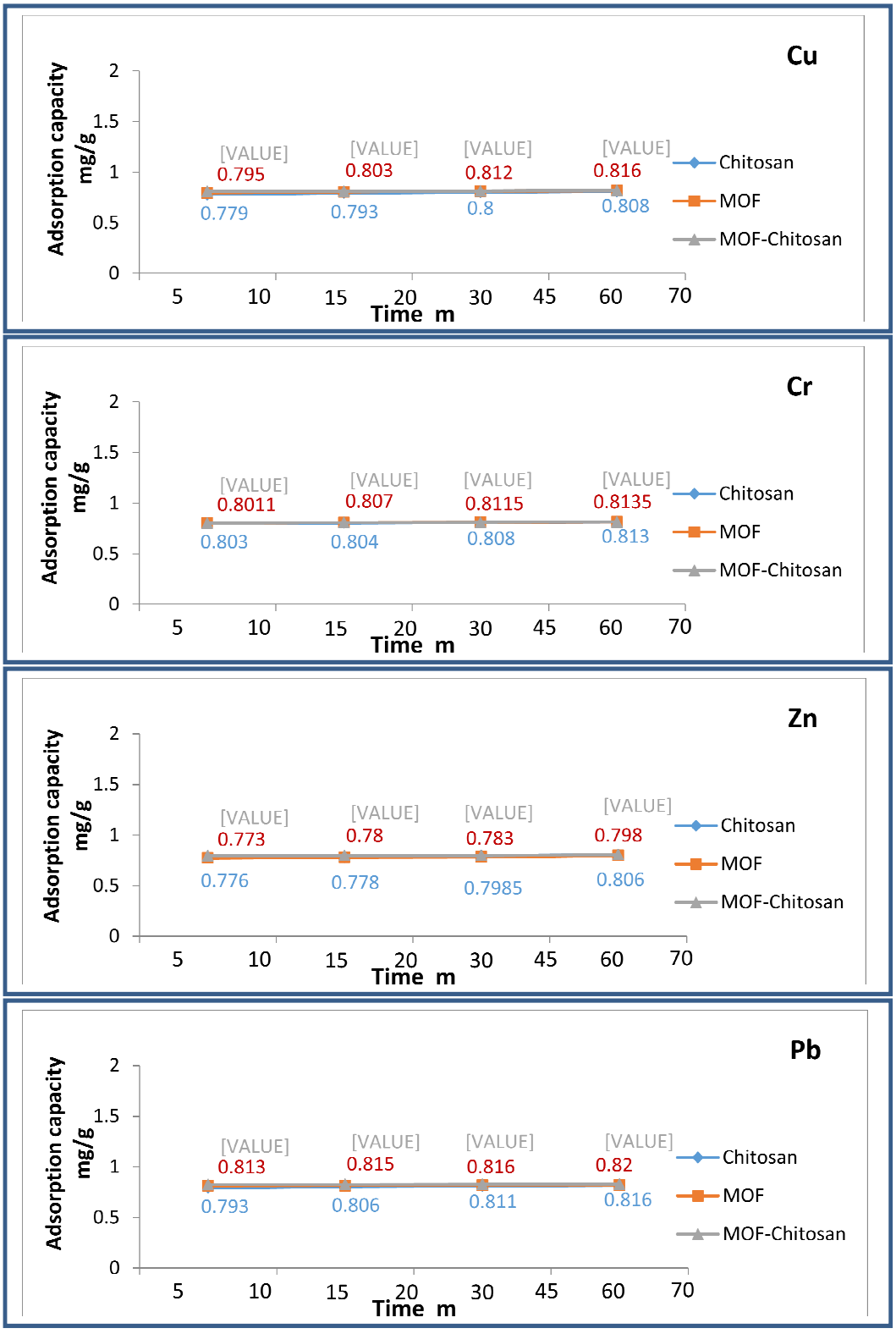

Fig. 30. Effect of contact time on adsorption capacity.

3.3. Adsorption isotherms

The adsorption behavior of Cu, Cr, Zn, and Pb was evaluated using both the Freundlich and Langmuir isotherm models, and the resulting parameters are shown in Figures 31–36. In the Freundlich model, the adsorption constants (Kf) for Cu, Cr, Zn, and Pb were found to vary across different adsorbents. Specifically, in Figure 31, Kf values were 1.2422, 0.3086, 0.48, and 1.8, with corresponding R^2 values of 0.7839, 0.8281, 0.8069, and 0.7951, indicating a moderate to good fit. In Figure 32, Kf values decreased to 0.209, 0.1259, 0.0228, and 0.1351, with improved R^2 values of 0.927, 0.9971, 0.8686, and 0.8194, respectively. Figure 33 continued this trend with Kf values of 0.1096, 0.1739, 0.0978, and 0.2567 and corresponding R^2 values of 0.8783, 0.9124, 0.9485, and 0.9994, indicating strong correlations and suggesting a good applicability of the Freundlich model.

In contrast, the Langmuir model yielded lower R^2 values in most cases. For instance, in Figure 34 (chitosan), the Langmuir constants (KL) were 0.1435, 0.0797, 0.0832, and 0.1851, but the R^2 values were considerably lower (0.2808 to 0.3819), suggesting poor fit. Figures 35 and 36 show some improvement in R^2 values (up to 0.9932 and 0.9943), but even in these cases, the Freundlich model often demonstrated a better overall correlation. This is particularly evident for Pb in Figure 33, which had a Freundlich R^2 of 0.9994, compared to a Langmuir R^2 of 0.7237 in Figure 36. Overall, the Freundlich model consistently showed higher R^2 values than the Langmuir model for all metals studied across the three adsorbents. This indicates that the Freundlich isotherm better represents the adsorption process, suggesting a heterogeneous surface with multilayer adsorption. Therefore, the adsorption of Cu, Cr, Zn, and Pb in this study is better described by the Freundlich model rather than the Langmuir model, which assumes monolayer adsorption on a homogeneous surface.

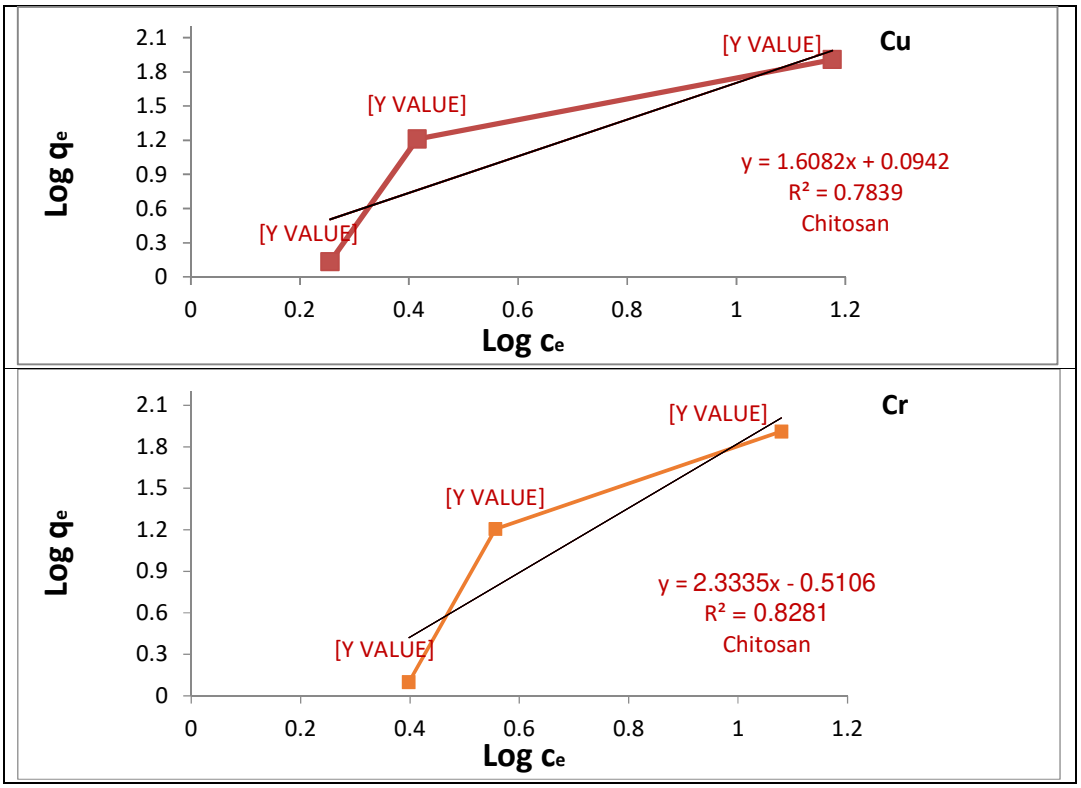

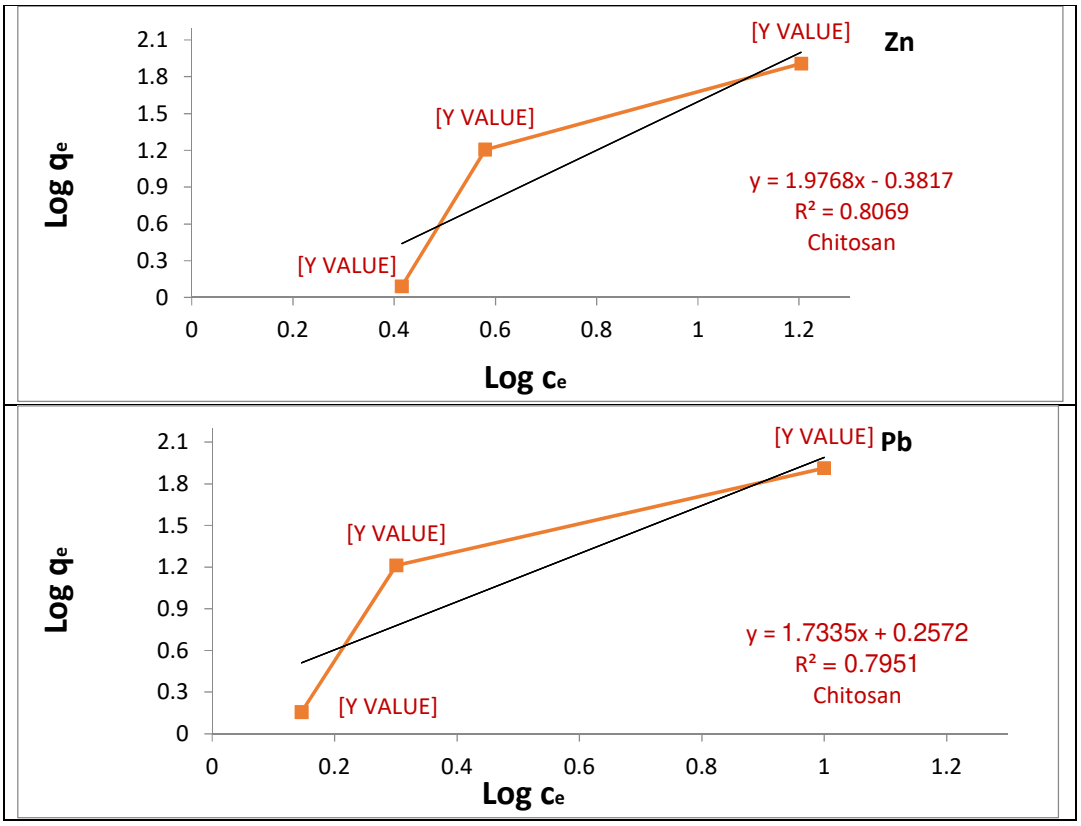

Fig. 31. Chitosan Freundlich isotherm plot for Cu, Cr, Zn and pb.

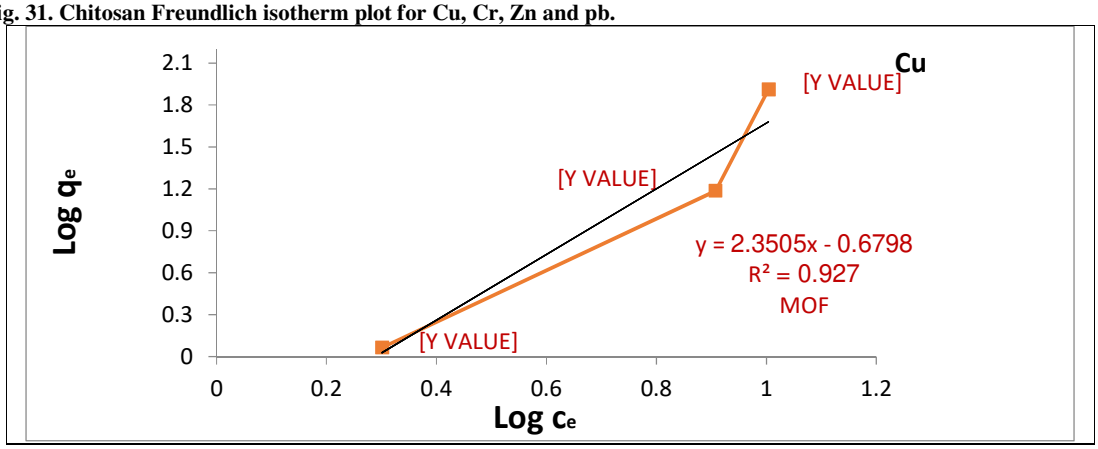

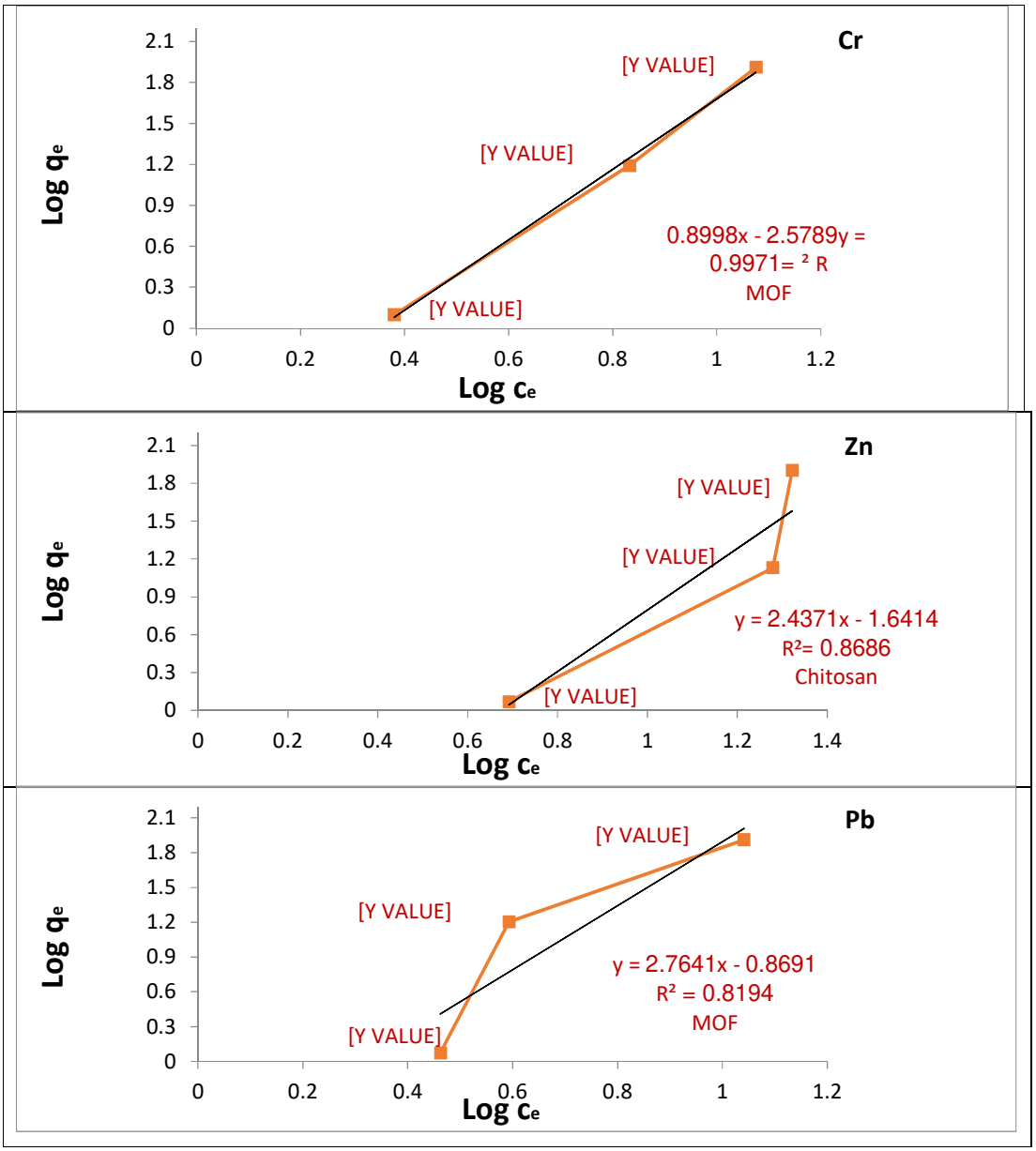

Fig. 32. MOF Freundlich isotherm plot for Cu, Cr, Zn and pb.

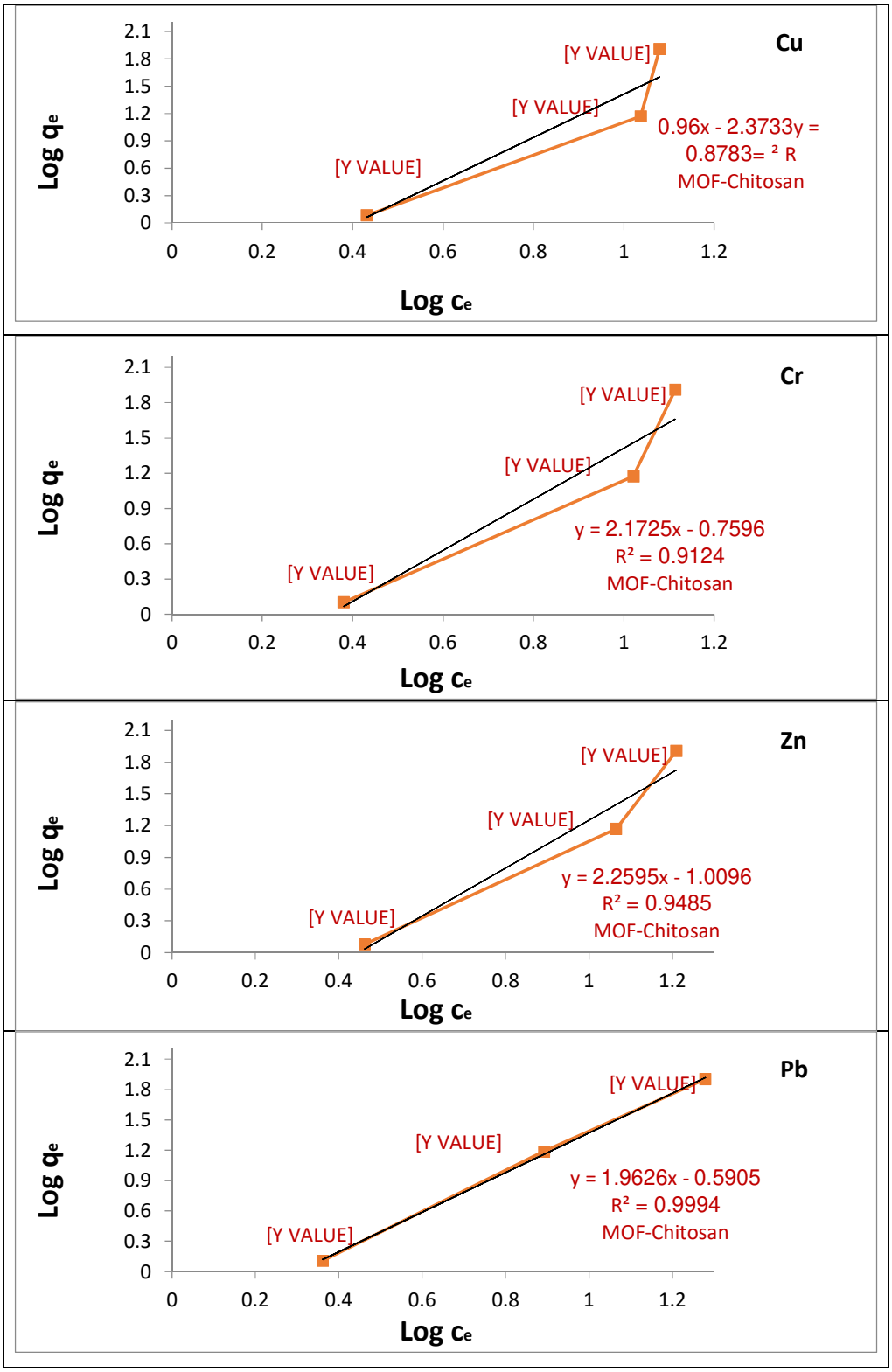

Fig. 33. Chitosan/MOF composite Freundlich isotherm plot for Cu, Cr, Zn and pb.

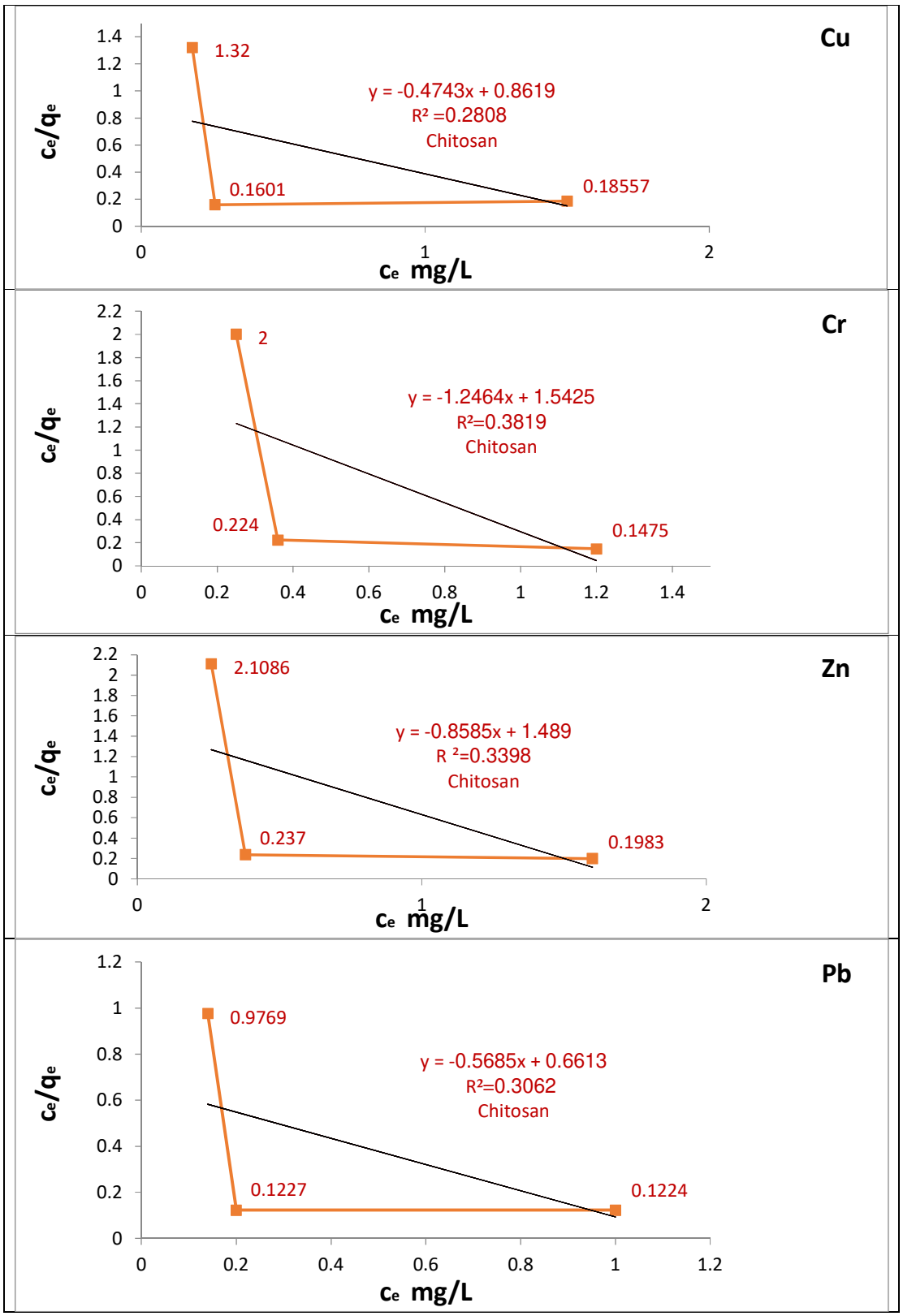

Fig. 34. Chitosan Langmuir isotherm plot for Cu, Cr, Zn and pb.

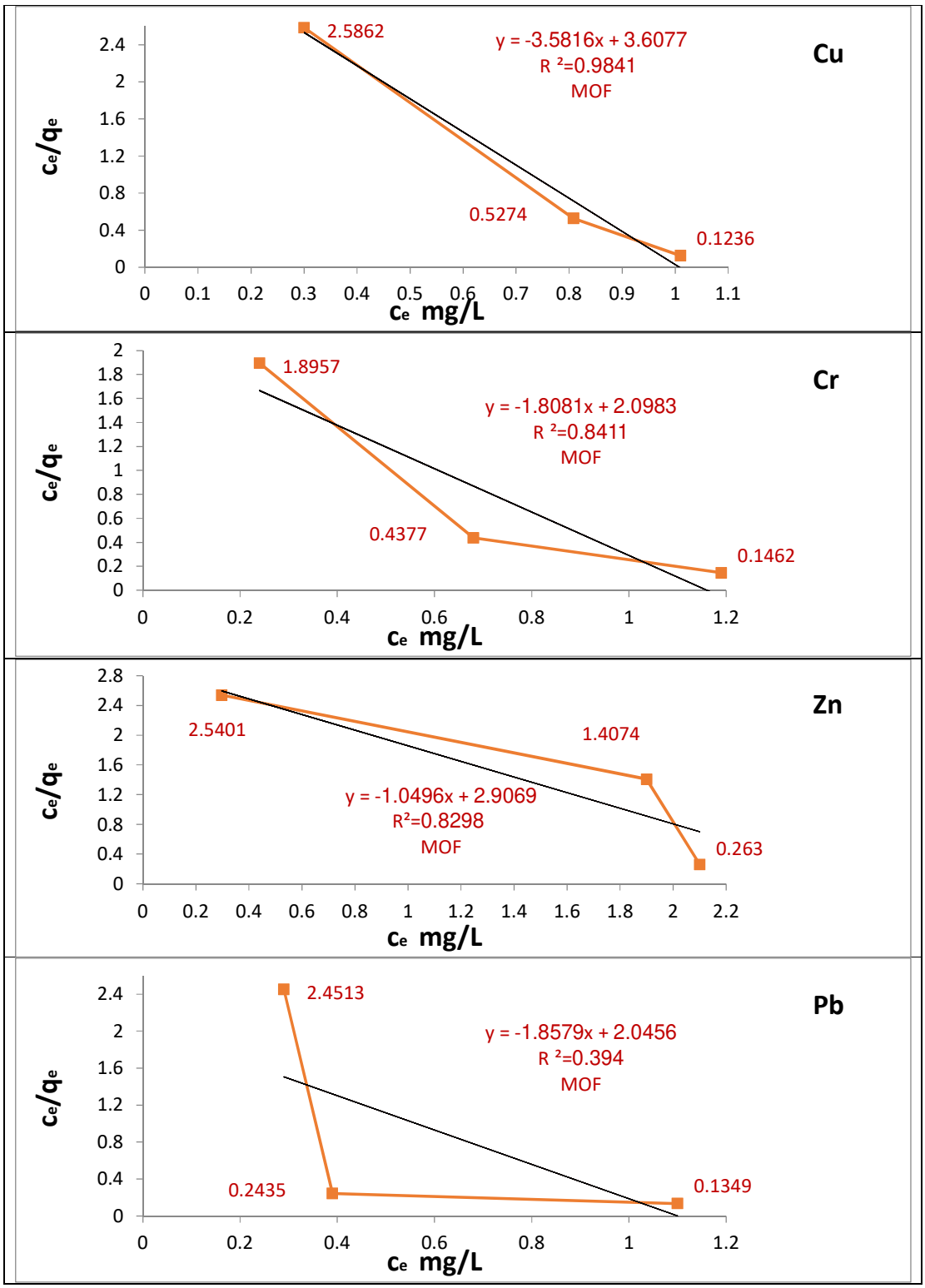

Fig. 35. MOF Langmuir isotherm plot for Cu, Cr, Zn and pb.

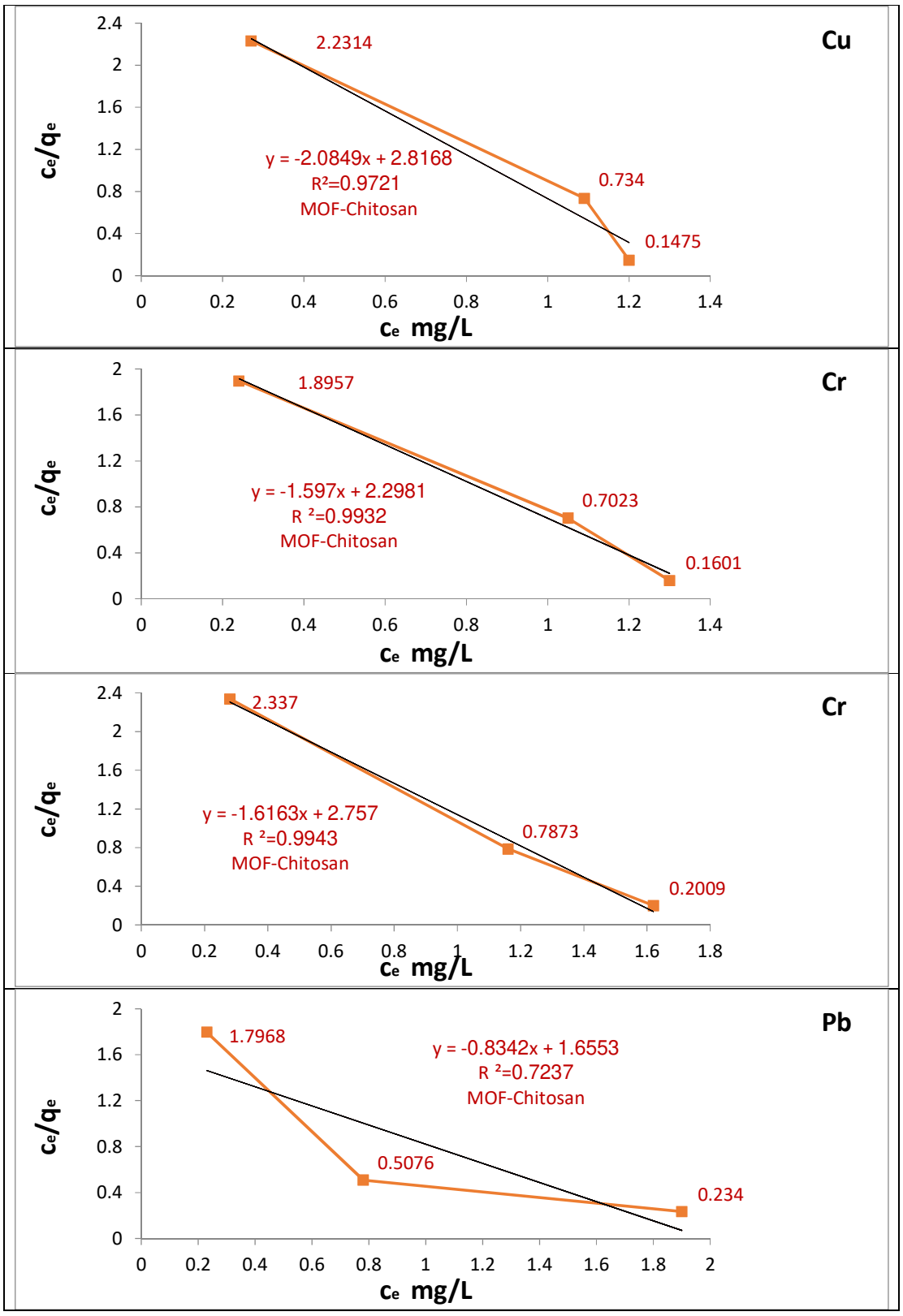

Fig. 36. Chitosan/MOF composite Langmuir isotherm plot for Cu, Cr, Zn and pb.

3.4. Comparison between chitosan, MOF and MOF/chitosan

This study presents the development and evaluation of a novel chitosan/MOF MIL(53) Fe composite for the efficient removal of heavy metals (Cu, Cr, Zn, and Pb) from wastewater. Compared to the individual components, the composite exhibits superior performance characterized by smaller particle size, significantly larger surface area (109.038 m^2/g), and higher adsorption capacity. The production technique for the chitosan/MOF composite is much less expensive than the separate expenses of chitosan and MOF in the worldwide market. The composite exhibits several advantages: smaller particle size, larger surface area, higher removal efficiency, and greater adsorption capacity than either chitosan or MOF alone, as detailed in Table 3. Given its superior qualities, the composite is extremely cost-effective, combining the benefits of chitosan and MOF. Isotherm modeling revealed a better fit to the Freundlich model, indicating multilayer adsorption on a heterogeneous surface. Biodegradation tests confirmed that chitosan decomposes within 14 days according to OECD guideline 301, while the MOF component can be regenerated via thermal (e.g., hot inert gas) or non-thermal methods (e.g., UV, microwave). MOF can be regenerated and reused through thermal and non-thermal methods. The thermal method involves using hot inert gas or steam, while the non-thermal method employs microwave heating, UV radiation, or electric currents [96]. The combination of chitosan's biodegradability and low cost with MOF's high porosity and tunable chemistry yields a stable, environmentally friendly, and scalable composite. The synthesis method is economical, pollutant-free, and suitable for large-scale application, making the composite a strong candidate for practical use in industrial wastewater treatment. In addition to confirming the composite's effectiveness, this work highlights its sustainability, cost-effectiveness, and potential for further optimization and real-world deployment.

Table 3: Comparison between chitosan, MOF, and MOF/chitosan composite

Items	**Chitosan**				**MOF**				**Chitosan/MOF composite**			
Manufacturing process price of (10) gram	It costs about (70) Egyptian pound for (10) g and (1100) Egyptian pound if we bought it from the market				It costs about (700) Egyptian pound for (10) g and (45000) Egyptian pound if we bought it from the market				It costs about (250) Egyptian pound for (10) g			
Average particles size	(50) nm				(50) nm				(20) nm			
Surface area	(16.5) m^2/g				(3.5) m^2/g				(109.038) m^2/g			
Removal % at pH 7	92.2	90.8	88.2	91.2	99.58	99.76	99.8	99.6	94.95	93.4	88.62	94.31
Adsorption capacity mg/g at pH 7	2.3	2.27	2.05	2.28	2.48	2.494	2.495	2.49	2.37	2.33	2.21	2.35
Removal efficiency % at 0.3 g	99.48	96.2	99.54	99.9	85.4	99.6	93	99.8	98.4	98.6	96.2	99.8
Adsorption capacity mg/g at 0.3 g	2.472	2.34	2.479	2.43	1.95	2.475	2.185	2.48	2.345	2.375	2.325	2.46
Removal efficiency % at 5 ppm	99.47	99.62	99.52	99.97	80.74	99.22	82.6	99.48	96.4	97.04	94.52	99.78
Adsorption capacity mg/g at 5 ppm	0.828	0.83	0.829	0.833	0.672	0.826	0.688	0.829	0.803	0.808	0.787	0.931
Removal efficiency % at 60 minutes	97	97.6	96.8	98	97.98	97.62	95.8	98.4	98.4	97.8	96.8	99.58
Adsorption capacity mg/g at 60 minutes	0.808	0.813	0.806	0.816	0.816	0.813	0.798	0.82	0.82	0.815	0.806	0.829
Freundlich adsorption constant k_f	1.242	0.308	0.48	1.8	0.209	0.125	0.022	0.135	0.109	0.173	0.097	0.2567
Freundlich Correlation coefficient R^2	0.783	0.828	0.806	0.795	0.927	0.997	0.868	0.819	0.878	0.912	0.948	0.9994

Langmuir adsorption constant k_L	0.143	0.079	0.083	0.185	0.033	0.05	0.043	0.059	0.043	0.053	0.044	0.0744
Langmuir Correlation coefficient R^2	0.280	0.381	0.339	0.306	0.984	0.841	0.829	0.394	0.972	0.993	0.994	0.7237

5. Future work

While the MOF MIL (53) Fe/chitosan composite has shown promising results in terms of surface area and heavy metal adsorption capacity, several avenues for future research could further enhance its performance and practical applicability. One potential direction involves optimizing the synthesis parameters—such as pH, temperature, and MOF-to-chitosan ratio—to achieve a more uniform distribution of active sites and improved structural stability. Additionally, incorporating functional groups (e.g., thiol, amine, or carboxyl) onto the composite surface could enhance selectivity and affinity toward specific heavy metal ions. Exploring the regeneration and reusability of the composite is also essential to assess its long-term operational feasibility in real-world water treatment systems. Moreover, performance evaluation under dynamic flow conditions, using actual industrial or municipal wastewater, would provide critical insights into scalability and real-life effectiveness. Finally, developing hybrid composites by integrating other materials, such as magnetic nanoparticles or carbon-based nanomaterials, may further improve separation efficiency, recyclability, and adsorption kinetics. These future improvements could pave the way for designing cost-effective, high-performance adsorbents tailored for a wide range of environmental remediation applications.

6. Conclusions

The goal of this article is to create chitosan, a metal-organic framework (MOF), and a chitosan/MOF composite and use them to remove copper, chromium, zinc, and lead from wastewater. The results showed that the three adsorbents' production techniques were effective. Chitosan, MOF, and chitosan/MOF composite had surface areas of 16.5, 3.5, and 109.038 m²/g, respectively. The particle sizes of chitosan, MOF, and the chitosan/MOF composite were 500–50 µm, 50–10 µm, and 500–50 µm, respectively. The production costs for 10 g of chitosan, MOF, and chitosan/MOF composite were around 70 Egyptian pounds, 700 Egyptian pounds, and 250 Egyptian pounds, respectively. The best results were obtained under the following conditions: pH 7, 0.3 g of adsorbent, a 5-ppm starting concentration, and a 60-minute contact duration. The mean removal efficiencies were 97.35% for chitosan, 97.45% for MOF, and 98.145% for the chitosan/MOF composite. The mean adsorption capacities were 0.81 mg/g for chitosan, 0.811 mg/g for MOF, and 0.817 mg/g for the chitosan/MOF composite. The chitosan/MOF composite had the best removal efficiency and adsorption capacity. Based on the isotherm data, the Freundlich isotherm model was shown to be more effective than the Langmuir isotherm model in removing copper, chromium, zinc, and lead from wastewater. In conclusion, the chitosan/MOF composite is a good adsorbent for removing heavy metals from wastewater due to its large surface area, great removal efficiency, superior adsorption capacity, and low manufacturing cost.

7. Conflicts of interest

Ther authors have no conflicts of interest to declare.

8. Funding sources

There are no external funding sources.

9. Acknowledgments

The authors are extremely thankful to the Technical Military College in Cairo and the Faculty of Engineering at Cairo University for their generous help.

10. References and Bibliography

[1] L. Lin, H. Yang, and X. Xu, "Effects of water pollution on human health and disease heterogeneity: a review," Frontiers in environmental science, vol. 10, p. 880246, 2022.
[2] W. Tang, Y. Pei, H. Zheng, Y. Zhao, L. Shu, and H. Zhang, "Twenty years of China's water pollution control: Experiences and challenges," Chemosphere, vol. 295, p. 133875, 2022.
[3] M. Roser, "Data review: how many people die from air pollution?" Our World in Data, 2023.
[4] W. H. Organization, Guidelines for drinking-water quality: incorporating the first and second addenda: World Health Organization, 2022.
[5] I. Priyadarshini, A. Alkhayyat, A. J. Obaid, and R. Sharma, "Water pollution reduction for sustainable urban development using machine learning techniques," Cities, vol. 130, p. 103970, 2022.
[6] J. Song, Y. Chen, and F. Luan, "Air pollution, water pollution, and robots: Is technology the panacea," Journal of Environmental Management, vol. 330, p. 117170, 2023.
[7] E. K. Nti, S. J. Cobbina, E. A. Attafuah, L. D. Senanu, G. Amenyeku, M. A. Gyan, et al., "Water pollution control and revitalization using advanced technologies: Uncovering artificial intelligence options towards environmental health protection, sustainability and water security," Heliyon, 2023.
[8] A. Pohl, "Removal of heavy metal ions from water and wastewaters by sulfur-containing precipitation agents," Water, Air, & Soil Pollution, vol. 231, p. 503, 2020.

[9] M. Bilal, I. Ihsanullah, M. Younas, and M. U. H. Shah, "Recent advances in applications of low-cost adsorbents for the removal of heavy metals from water: A critical review," Separation and Purification Technology, vol. 278, p. 119510, 2021.
[10] V. Kumar, R. D. Parihar, A. Sharma, P. Bakshi, G. P. S. Sidhu, A. S. Bali, et al., "Global evaluation of heavy metal content in surface water bodies: A meta-analysis using heavy metal pollution indices and multivariate statistical analyses," Chemosphere, vol. 236, p. 124364, 2019.
[11] Q. Zhou, N. Yang, Y. Li, B. Ren, X. Ding, H. Bian, et al., "Total concentrations and sources of heavy metal pollution in global river and lake water bodies from 1972 to 2017," Global Ecology and Conservation, vol. 22, p. e00925, 2020.
[12] Z. Fu and S. Xi, "The effects of heavy metals on human metabolism," Toxicology mechanisms and methods, vol. 30, pp. 167-176, 2020.
[13] M. K. Abd Elnabi, N. E. Elkaliny, M. M. Elyazied, S. H. Azab, S. A. Elkhalifa, S. Elmasry, et al., "Toxicity of heavy metals and recent advances in their removal: A review," Toxics, vol. 11, p. 580, 2023.
[14] R. N. Khalef, A. I. Hassan, and H. M. Saleh, "Heavy metal's environmental impact," 2022.
[15] R. Abedi Sarvestani and M. Aghasi, "Health risk assessment of heavy metals exposure (lead, cadmium, and copper) through drinking water consumption in Kerman city, Iran," Environmental earth sciences, vol. 78, pp. 1-11, 2019.
[16] R. N. Khalef, A. I. Hassan, and H. M. Saleh, "Heavy Metal's Environmental Impact," in Environmental Impact and Remediation of Heavy Metals, ed: IntechOpen, 2022.
[17] S. S. Sonone, S. Jadhav, M. S. Sankhla, and R. Kumar, "Water contamination by heavy metals and their toxic effect on aquaculture and human health through food Chain," Lett. Appl. NanoBioScience, vol. 10, pp. 2148-2166, 2020.
[18] A. C. Olufemi, A. Mji, and M. S. Mukhola, "Potential health risks of lead exposure from early life through later life: implications for public health education," International Journal of Environmental Research and Public Health, vol. 19, p. 16006, 2022.
[19] T. A. Saleh, M. Mustaqeem, and M. Khaled, "Water treatment technologies in removing heavy metal ions from wastewater: A review," Environmental Nanotechnology, Monitoring & Management, vol. 17, p. 100617, 2022.
[20] A. J. dos Santos, H. L. Barazorda-Ccahuana, G. Caballero-Manrique, Y. Chérémond, P. J. Espinoza-Montero, J. R. González-Rodríguez, et al., "Accelerating innovative water treatment in Latin America," Nature Sustainability, vol. 6, pp. 349-351, 2023.
[21] N. A. Qasem, R. H. Mohammed, and D. U. Lawal, "Removal of heavy metal ions from wastewater: A comprehensive and critical review," Npj Clean Water, vol. 4, p. 36, 2021.
[22] S. S. Dhaliwal, J. Singh, P. K. Taneja, and A. Mandal, "Remediation techniques for removal of heavy metals from the soil contaminated through different sources: a review," Environmental Science and Pollution Research, vol. 27, pp. 1319-1333, 2020.
[23] R. Shrestha, S. Ban, S. Devkota, S. Sharma, R. Joshi, A. P. Tiwari, et al., "Technological trends in heavy metals removal from industrial wastewater: A review," Journal of Environmental Chemical Engineering, vol. 9, p. 105688, 2021.
[24] F. S. A. Khan, N. M. Mubarak, M. Khalid, R. Walvekar, E. C. Abdullah, S. A. Mazari, et al., "Magnetic nanoadsorbents' potential route for heavy metals removal—a review," Environmental Science and Pollution Research, vol. 27, pp. 24342-24356, 2020.
[25] Y. Fei and Y. H. Hu, "Recent progress in removal of heavy metals from wastewater: A comprehensive review," Chemosphere, p. 139077, 2023.
[26] P. Jiamjirangkul, T. Inprasit, V. Intasanta, and A. Pangon, "Metal organic framework-integrated chitosan/poly (vinyl alcohol)(PVA) nanofibrous membrane hybrids from green process for selective CO2 capture and filtration," Chemical Engineering Science, vol. 221, p. 115650, 2020.
[27] J. Farahbakhsh, M. Najafi, M. Golgoli, A. H. Asif, M. Khiadani, A. Razmjou, et al., "Microplastics and Dye Removal from Textile Wastewater Using MIL-53 (Fe) Metal-Organic Framework-based Ultrafiltration Membranes," Chemosphere, p. 143170, 2024.
[28] S. Darvishi, S. Sadjadi, and M. M. Heravi, "Sulfonic acid-functionalized chitosan–metal–organic framework composite for efficient and rapid conversion of fructose to 5-hydroxymethylfurfural," Scientific Reports, vol. 14, p. 5834, 2024.
[29] I. Ghaffar, M. Imran, S. Perveen, T. Kanwal, S. Saifullah, M. F. Bertino, et al., "Synthesis of chitosan coated metal organic frameworks (MOFs) for increasing vancomycin bactericidal potentials against resistant S. aureus strain," Materials Science and Engineering: C, vol. 105, p. 110111, 2019.
[30] I. Salahshoori, M. N. Jorabchi, S. Ghasemi, M. Golriz, S. Wohlrab, and H. A. Khonakdar, "Advancements in wastewater Treatment: A computational analysis of adsorption characteristics of cationic dyes pollutants on amide Functionalized-MOF nanostructure MIL-53 (Al) surfaces," Separation and Purification Technology, vol. 319, p. 124081, 2023.
[31] K. Poonia, S. Patial, P. Raizada, T. Ahamad, A. A. P. Khan, Q. Van Le, et al., "Recent advances in Metal Organic Framework (MOF)-based hierarchical composites for water treatment by adsorptional photocatalysis: A review," Environmental Research, p. 115349, 2023.
[32] Y. Yao, C. Wang, J. Na, M. S. A. Hossain, X. Yan, H. Zhang, et al., "Macroscopic MOF architectures: Effective strategies for practical application in water treatment," Small, vol. 18, p. 2104387, 2022.
[33] Y. Jin, Y. Li, Q. Du, B. Chen, K. Chen, Y. Zhang, et al., "Efficient adsorption of Congo red by MIL-53 (Fe)/chitosan composite hydrogel spheres," Microporous and Mesoporous Materials, vol. 348, p. 112404, 2023.
[34] X. Yan and H. Ge, "Preparation of metal organic frameworks modified chitosan composite with high capacity for Hg (II) adsorption," International Journal of Biological Macromolecules, vol. 232, p. 123329, 2023.
[35] Z.-S. Zhao, Y. Zhang, T. Fang, Z.-B. Han, and F.-S. Liang, "Chitosan-coated metal–organic-framework nanoparticles as catalysts for tandem Deacetalization–Knoevenagel condensation reactions," ACS Applied Nano Materials, vol. 3, pp. 6316-6320, 2020.

[36] H. Selvaraj, K. Periyannan, and S. Balachandar, "Extraction and Characterization of Chitosan from the Shell Wastes of Indian Shrimp Using Different Methods of Deacetylation," Indian Journal of Science and Technology, vol. 16, pp. 1118-1125, 2023.
[37] N. Boudouaia, Z. Bengharez, and S. Jellali, "Preparation and characterization of chitosan extracted from shrimp shells waste and chitosan film: application for Eriochrome black T removal from aqueous solutions," Applied Water Science, vol. 9, p. 91, 2019.
[38] A. M. Sixto-Berrocal, M. Vázquez-Aldana, S. P. Miranda-Castro, M. A. Martínez-Trujillo, and M. R. Cruz-Díaz, "Chitin/chitosan extraction from shrimp shell waste by a completely biotechnological process," International Journal of Biological Macromolecules, vol. 230, p. 123204, 2023.
[39] P. Dinh Du and P. Ngoc Hoai, "Synthesis of MIL-53 (Fe) metal-organic framework material and its application as a catalyst for Fenton-type oxidation of organic pollutants," Advances in Materials Science and Engineering, vol. 2021, pp. 1-13, 2021.
[40] S. Tomar and V. Singh, "Review on synthesis and application of MIL-53," Materials Today: Proceedings, vol. 43, pp. 3291-3296, 2021.
[41] A. Balakrishnan, M. M. Jacob, N. Dayanandan, M. Chinthala, M. Ponnuchamy, D.-V. N. Vo, et al., "Chitosan/metal organic frameworks for environmental, energy, and bio-medical applications: a review," Materials Advances, 2023.
[42] J. Xiao, Y. Song, and Y. Li, "Comparison of Quantitative X-ray Diffraction Mineral Analysis Methods," Minerals, vol. 13, p. 566, 2023.
[43] V.-A. Surdu and R. Győrgy, "X-ray Diffraction Data Analysis by Machine Learning Methods—A Review," Applied Sciences, vol. 13, p. 9992, 2023.
[44] S. Iram, M. Imran, F. Kanwal, S. Latif, and Z. Iqbal, "Bismuth and lead based metal organic frameworks: morphological, luminescence and brunauer-emmett-teller (BET) studies," Materials Science-Poland, vol. 38, pp. 132-137, 2020.
[45] R. Bardestani, G. S. Patience, and S. Kaliaguine, "Experimental methods in chemical engineering: specific surface area and pore size distribution measurements—BET, BJH, and DFT," The Canadian Journal of Chemical Engineering, vol. 97, pp. 2781-2791, 2019.
[46] L.-C. Fengou, E. Spyrelli, A. Lianou, P. Tsakanikas, E. Z. Panagou, and G.-J. E. Nychas, "Estimation of minced pork microbiological spoilage through Fourier transform infrared and visible spectroscopy and multispectral vision technology," Foods, vol. 8, p. 238, 2019.
[47] B. Kaźmierczak, J. Molenda, and M. Swat, "The adsorption of chromium (III) ions from water solutions on biocarbons obtained from plant waste," Environmental Technology & Innovation, vol. 23, p. 101737, 2021.
[48] M. Slouf, R. Skoupy, E. Pavlova, and V. Krzyzanek, "High resolution powder electron diffraction in scanning electron microscopy," Materials, vol. 14, p. 7550, 2021.
[49] A. Wurm, J. Kühn, K. Kugel, D. Putzer, R. Arora, D. Coraça-Huber, et al., "Raman microscopic spectroscopy as a diagnostic tool to detect Staphylococcus epidermidis in bone grafts," Spectrochimica Acta Part A: Molecular and Biomolecular Spectroscopy, vol. 280, p. 121570, 2022.
[50] K. Li, Y. Bu, and H. Wang, "Advances on in situ TEM mechanical testing techniques: a retrospective and perspective view," Frontiers in Materials, vol. 10, p. 1207024, 2023.
[51] H. Wu, H. Su, R. R. Joosten, A. D. Keizer, L. S. van Hazendonk, M. J. Wirix, et al., "Mapping and Controlling Liquid Layer Thickness in Liquid-Phase (Scanning) Transmission Electron Microscopy," Small Methods, vol. 5, p. 2001287, 2021.
[52] D. Vicente-Zurdo, B. Gómez-Gómez, I. Romero-Sánchez, N. Rosales-Conrado, M. E. León-González, and Y. Madrid, "Cytotoxicity, uptake and accumulation of selenium nanoparticles and other selenium species in neuroblastoma cell lines related to Alzheimer's disease by using cytotoxicity assays, TEM and single cell-ICP-MS," Analytica Chimica Acta, vol. 1249, p. 340949, 2023.
[53] S. Albukhaty, L. Al-Bayati, H. Al-Karagoly, and S. Al-Musawi, "Preparation and characterization of titanium dioxide nanoparticles and in vitro investigation of their cytotoxicity and antibacterial activity against Staphylococcus aureus and Escherichia coli," Animal Biotechnology, vol. 33, pp. 864-870, 2022.
[54] J. Ogana, I. Usman, T. Akpa, S. Yusuf, U. Gurku, and U. Ibrahim, "Inductively coupled plasma mass spectrometry (ICP-MS): A modern analytical technique for nuclear forensic application," Dutse J Pure Applied Sci, vol. 5, pp. 231-9, 2019.
[55] D. Das and D. Das, "Biosorption Kinetics," Biochemical Engineering: A Laboratory Manual, p. 171, 2021.
[56] M. Sharma, V. Singh, and R. Devi, "Removal of Cd 2 from synthetic solution by using leaves of Neem, Peepal and Mixed adsorbent."
[57] T. S. Khayyun and A. H. Mseer, "Comparison of the experimental results with the Langmuir and Freundlich models for copper removal on limestone adsorbent," Applied Water Science, vol. 9, p. 170, 2019.
[58] R. A. Mansour, N. M. Aboeleneen, and Nabil M. AbdelMonem, "Adsorption of cationic dye from aqueous solutions by date pits: Equilibrium, kinetic, thermodynamic studies, and batch adsorber design." International journal of phytoremediation vol. 20, p. 1062-1074, 2018.
[59] S. Farhadi, M. R. Sohrabi, F. Motiee, and M. Davallo, "Organophosphorus diazinon pesticide removing from aqueous solution by zero-valent iron supported on biopolymer chitosan: RSM optimization methodology," Journal of Polymers and the Environment, vol. 29, pp. 103-120, 2021.
[60] M. Rabiei, A. Palevicius, A. Monshi, S. Nasiri, A. Vilkauskas, and G. Janusas, "Comparing methods for calculating nano crystal size of natural hydroxyapatite using X-ray diffraction," Nanomaterials, vol. 10, p. 1627, 2020.
[61] T. Sirijaree and P. Praipipat, "Adsorption of Lead (II) Ions onto Goethite Chitosan Beads: Isotherms, Kinetics, and Mechanism Studies," ChemEngineering, vol. 7, p. 52, 2023.
[62] A. A. Pam, O. O. Elemile, D. E. Musa, M. C. Okere, A. Olusegun, and Y. A. Ameh, "Removal of Cu (II) via chitosan-conjugated iodate porous adsorbent: Kinetics, thermodynamics, and exploration of real wastewater sample," Results in Chemistry, vol. 5, p. 100851, 2023.

[63]Z. Yang, Y. Chai, L. Zeng, Z. Gao, J. Zhang, and H. Ji, "Efficient removal of copper ion from wastewater using a stable chitosan gel material," Molecules, vol. 24, p. 4205, 2019.
[64]M. A. Akl, A. G. Mostafa, M. Y. Abdelaal, and M. A. K. Nour, "Surfactant supported chitosan for efficient removal of Cr (VI) and anionic food stuff dyes from aquatic solutions," Scientific Reports, vol. 13, p. 15786, 2023.
[65]A. Pooladi and R. Bazargan-Lari, "Simultaneous removal of copper and zinc ions by Chitosan/Hydroxyapatite/nano-Magnetite composite," Journal of Materials Research and Technology, vol. 9, pp. 14841-14852, 2020.
[66]P. Ngamsurach, N. Namwongsa, and P. Praipipat, "Synthesis of powdered and beaded chitosan materials modified with ZnO for removing lead (II) ions," Scientific Reports, vol. 12, p. 17184, 2022.
[67]X. Yang, H. Zhang, S. Cheng, and B. Zhou, "Optimization of the adsorption and removal of Sb (iii) by MIL-53 (Fe)/GO using response surface methodology," RSC advances, vol. 12, pp. 4101-4112, 2022.
[68]M. Ghanbarian, S. Zeinali, A. Mostafavi, and T. Shamspur, "Facile synthesis of MIL-53 (Fe) by microwave irradiation and its application for robust removal of heavy metals from aqueous solution by experimental design approach: Kinetic and equilibrium," Analytical and Bioanalytical Chemistry Research, vol. 7, pp. 263-280, 2020.
[69]S. Duan, Y. Gao, G. Lan, H. Qiu, B. Xu, Z. Xie, et al., "In-situ synthesis of MIL-100 (Fe)@ chitosan composite beads with hierarchical porous structure for efficient adsorption of chlortetracycline hydrochloride: Synthesis, performance and mechanisms," Separation and Purification Technology, p. 125938, 2023.
[70]B. Zhang, L. Zhang, K. Akiyama, P. A. Bingham, Y. Zhou, and S. Kubuki, "Self-assembly of nanosheet-supported Fe-MOF heterocrystals as a reusable catalyst for boosting advanced oxidation performance via radical and nonradical pathways," ACS Applied Materials & Interfaces, vol. 13, pp. 22694-22707, 2021.
[71]M. Eddya, B. Tbib, and E.-H. Khalil, "A comparison of chitosan properties after extraction from shrimp shells by diluted and concentrated acids," Heliyon, vol. 6, 2020.
[72]E. O. Babatunde, J. O. Ighalo, S. A. Akolo, A. G. Adeniyi, and L. Adepoju, "Investigation of biomaterial characteristics of chitosan produced from crab shells," 2020.
[73]H. V. Tran, H. T. M. Dang, L. T. Tran, C. Van Tran, and C. D. Huynh, "Metal-organic framework MIL-53 (Fe): synthesis, electrochemical characterization, and application in development of a novel and sensitive electrochemical sensor for detection of cadmium ions in aqueous solutions," Advances in Polymer Technology, vol. 2020, pp. 1-10, 2020.
[74] Atef, Riham, N. M. Aboeleneen, and Nabil M. AbdelMonem. "Preparation and characterization of low-cost nano-particle material using pomegranate peels for brilliant green removal." International Journal of Phytoremediation vol. 25. p. 36-46, 2023.
[75] Sorour, Faisal Hassan, et al. "Removal of malachite green from wastewater using date seeds as natural adsorbent; isotherms, kinetics, Thermodynamic, and batch adsorption process design." International Journal of Phytoremediation p. 1-15, 2024.
[76]C. M. Navarathna, N. B. Dewage, A. G. Karunanayake, E. L. Farmer, F. Perez, E. B. Hassan, et al., "Rhodamine B adsorptive removal and photocatalytic degradation on MIL-53-Fe MOF/magnetic magnetite/biochar composites," Journal of Inorganic and Organometallic Polymers and Materials, vol. 30, pp. 214-229, 2020.
[77]R. Varma and S. Vasudevan, "Extraction, characterization, and antimicrobial activity of chitosan from horse mussel modiolus," ACS omega, vol. 5, pp. 20224-20230, 2020.
[78]J. López, A. M. Chávez, A. Rey, and P. M. Álvarez, "Insights into the stability and activity of MIL-53 (Fe) in solar photocatalytic oxidation processes in water," Catalysts, vol. 11, p. 448, 2021.
[79]R. Nivetha, P. Kollu, K. Chandar, S. Pitchaimuthu, S. K. Jeong, and A. N. Grace, "Role of MIL-53 (Fe)/hydrated–dehydrated MOF catalyst for electrochemical hydrogen evolution reaction (HER) in alkaline medium and photocatalysis," RSC advances, vol. 9, pp. 3215-3223, 2019.
[80]E. M. Abd El-Monaem, A. M. Omer, and A. S. Eltaweil, "Durable and Low-Cost Chitosan Decorated Fe/MOF-5 Bimetallic MOF Composite Film for High Performance of the Congo Red Adsorption," Journal of Polymers and the Environment, pp. 1-16, 2023.
[81]C. Zanca, B. Patella, E. Capuana, F. Lopresti, V. Brucato, F. Carfì Pavia, et al., "Behavior of Calcium Phosphate–Chitosan–Collagen Composite Coating on AISI 304 for Orthopedic Applications," Polymers, vol. 14, p. 5108, 2022.
[82]J. Jayanudin, R. S. Lestari, I. Kustiningsih, D. Irawanto, R. Rozak, R. L. Wardana, et al., "Sustainable material for urea delivery based on chitosan cross-linked by glutaraldehyde saturated toluene: Characterization and determination of the release rate mathematical model," Karbala International Journal of Modern Science, vol. 8, pp. 657-669, 2022.
[83]B. Gieroba, A. Sroka-Bartnicka, P. Kazimierczak, G. Kalisz, A. Lewalska-Graczyk, V. Vivcharenko, et al., "Surface chemical and morphological analysis of chitosan/1, 3-β-d-glucan polysaccharide films cross-linked at 90° C," International Journal of Molecular Sciences, vol. 23, p. 5953, 2022.
[84]T. V. Tran, D. T. C. Nguyen, H. T. Le, L. G. Bach, D.-V. N. Vo, K. T. Lim, et al., "Combined minimum-run resolution IV and central composite design for optimized removal of the tetracycline drug over metal–organic framework-templated porous carbon," Molecules, vol. 24, p. 1887, 2019.
[85]D. T. C. Nguyen, H. T. N. Le, T. S. Do, V. T. Pham, L. Dai Tran, V. T. T. Ho, et al., "Metal-organic framework MIL-53 (Fe) as an adsorbent for ibuprofen drug removal from aqueous solutions: response surface modeling and optimization," Journal of Chemistry, vol. 2019, 2019.
[86]T. Van Tran, D. T. Cam Nguyen, H. T. Le, O. T. Nguyen, V. H. Nguyen, T. T. Nguyen, et al., "A hollow mesoporous carbon from metal-organic framework for robust adsorbability of ibuprofen drug in water," Royal Society open science, vol. 6, p. 190058, 2019.
[87]M. A. A. H. Allah and H. A. Alshamsi, "Green Synthesis of ZnO Coated Porous Activated Carbon Prepared from Pontederia crassipe Leaves for the Adsorptive Removal of Toxic Organic Dyes," 2023.

[88] D. D. Kachhadiya and Z. Murthy, "Highly efficient chitosan-based bio-polymeric membranes embedded with green solvent encapsulated MIL-53 (Fe) for methanol/MTBE separation by pervaporation," Journal of Environmental Chemical Engineering, vol. 11, p. 109307, 2023.
[89] E. Mirda, R. Idroes, K. Khairan, T. E. Tallei, M. Ramli, N. Earlia, et al., "Synthesis of chitosan-silver nanoparticle composite spheres and their antimicrobial activities," Polymers, vol. 13, p. 3990, 2021.
[90] C. N. Lunardi, A. J. Gomes, F. S. Rocha, J. De Tommaso, and G. S. Patience, "Experimental methods in chemical engineering: Zeta potential," The Canadian Journal of Chemical Engineering, vol. 99, pp. 627-639, 2021.
[91] J. Li, C. Yu, Y.-n. Wu, Y. Zhu, J. Xu, Y. Wang, et al., "Novel sensing platform based on gold nanoparticle-aptamer and Fe-metal-organic framework for multiple antibiotic detection and signal amplification," Environment international, vol. 125, pp. 135-141, 2019.
[92] C. Ardean, C. M. Davidescu, N. S. Nemeş, A. Negrea, M. Ciopec, N. Duteanu, et al., "Factors influencing the antibacterial activity of chitosan and chitosan modified by functionalization," International Journal of Molecular Sciences, vol. 22, p. 7449, 2021.
[93] Sorour, Faisal Hassan, et al. "Raw sawdust utilization for the removal of acid red57 and basic fuchsin dyes from aqueous solution: equilibrium, kinetics, and thermodynamic investigation." International Journal of Phytoremediation vol. 26, p. 669-683, 2024.
[94] M. E. Peralta, R. Nisticò, F. Franzoso, G. Magnacca, L. Fernandez, M. E. Parolo, et al., "Highly efficient removal of heavy metals from waters by magnetic chitosan-based composite," Adsorption, vol. 25, pp. 1337-1347, 2019.
[95] Aboeleneen, N. M., Nabil M. AbdelMonem, and Riham Atef. "Effective application of green nano adsorbent on the removal of carbofuran from wastewater." Chemical Engineering Communications vol. 212, p. 235-249, 2025.
[96] L. Hashemi, M. Y. Masoomi, and H. Garcia, "Regeneration and reconstruction of metal-organic frameworks: Opportunities for industrial usage," Coordination Chemistry Reviews, vol. 472, p. 214776, 2022.